EFEMP1 contributes to light-dependent ocular growth in zebrafish

Jiaheng Xie[1], Bang V. Bui[2], Patrick T. Goodbourn[3], Patricia R. Jusuf[1]*

[1] School of Biosciences, The University of Melbourne
[2] Department of Optometry and Vision Sciences, The University of Melbourne
[3] Melbourne School of Psychological Sciences, The University of Melbourne
*patricia.jusuf@unimelb.edu.au

Abstract

Myopia (short-sightedness) is the most common ocular disorder. It generally develops after over-exposure to aberrant visual environments, disrupting emmetropization mechanisms that should match eye growth with optical power. A pre-screening of strongly associated myopia-risk genes identified through human genome-wide association studies implicates *efemp1* in myopia development, but how this gene impacts ocular growth remains unclear. Here, we modify *efemp1* expression specifically in the retina of zebrafish. We found that under normal lighting, *efemp1* mutants developed axial myopia, enlarged eyes, reduced spatial vision and altered retinal function. However, under myopia-inducing dark-rearing, compared to control fish, mutants remained emmetropic and showed changes in retinal function. *Efemp1* modification changed the expression of *efemp1*, *egr1*, *tgfb1a*, *vegfab* and *rbp3* genes in the eye, and changes the inner retinal distributions of myopia-associated EFEMP1, TIMP2 and MMP2 proteins. *Efemp1* modification also impacted dark-rearing-induced responses of *vegfab* and *wnt2b* genes and above-mentioned myopia-associated proteins. Together, we provided robust evidence that light-dependent ocular growth is regulated by *efemp1*.

Summary

This study shows that retina-specific modification of *efemp1* expression in zebrafish results in myopic eye, and impacts responses to myopia-inducing dark-rearing in eye growth, retinal function, and myopia-associated molecular expression and distribution, implicating light-dependent regulation of *efemp1* in ocular development.

Introduction

Myopia (short-sightedness) is now the most common visual disorder, and is predicted to impact approximately half of the world population by 2050 (Holden et al., 2016). Although considered manageable with optical correction, the development of high levels of myopia (or pathological myopia) brings with it ocular changes that promote eye diseases that cannot be easily managed (glaucoma, cataract, myopic maculopathy, etc.) (Hayashi et al., 2010; Ikuno, 2017; Marcus et al., 2011). Thus, there is an urgent need to better understand this condition.

During development, emmetropization mechanisms use visual cues to regulate eye growth, in order to match eye size with its optic power, to achieve focused vision (Rabin et al., 1981). Extended exposure to aberrant visual environments can lead to dysregulation of emmetropization mechanisms resulting in myopia. Human studies showed that children who spent more time outdoors were less likely to develop myopia (Rose et al., 2008). Recent shifts away from outdoor activities and increased screen time may further increase myopia prevalence and promote pathological myopia (Najafzadeh et al., 2023). This points to an urgent need to understand the underlying mechanisms for myopia development, to underpin the development of novel approaches to target these mechanisms.

A range of myopia-associated genes have been identified over the past several decades (Tedja et al., 2019). Meta-analyses of an increasingly large pool of human genome-wide association (GWAS) data have seen a growth in the number of novel risk genes associated with refractive error (Tedja et al., 2018). Amongst the highest ranked myopia risk genes is *EGF containing fibulin extracellular matrix protein 1* (*efemp1*). EFEMP1 is a secreted extracellular matrix glycoprotein widely expressed throughout the human body, especially in elastic fiber-rich tissues, for examples, the brain, lung, kidney and eye including the retina (Livingstone et al., 2020; Mackay et al., 2015). Our previous study (unpublished) screening GWAS-associated myopia-risk genes with high-throughput optomotor response measurement and morpholino gene knockdown indicated that knockdown of *efemp1* in larval zebrafish reduced spatial-frequency tuning function, making *efemp1* a candidate gene worth for further investigation for myopia development. In relation to human visual diseases, an autosomal dominant gain-of-function mutation in the *EFEMP1* gene (c.1033C>T, p.Arg345Trp) is known to be associated

with Malattia Leventinese and Doyne honeycomb retinal dystrophy (Stone et al., 1999), leading to accumulation of drusen (yellow-white deposits) beneath the basal retinal pigment epithelium (RPE), a pathologic sign that overlaps with age-related macular degeneration (AMD) (Marmorstein et al., 2002). A number of studies suggest that sub-RPE deposits may result from abnormal interactions between EFEMP1 and complement system proteins, for example, complement component 3 (C3), complement factor B (FB) and complement factor H (CFH) (Crowley et al., 2022; Garland et al., 2013).

Recently, from 3 independent Filipino families, three novel *EFEMP1* variants (c.238A>T, p.Asn80Tyr; c.1480T>C, p.Ter494Glnext*29; and c.1429C>T, p.Arg477Cys) were identified in patients with juvenile-onset open-angle glaucoma, in which 76% of the carriers eventually developed blindness (Collantes et al., 2022). This study also demonstrated that protein aggregation and retention was the potential cause of juvenile-onset open-angle glaucoma. In addition, a recent reported case with biallelic *EFEMP1* loss-of-function variants (c.320_324del, p.Met107fs; c.615T>A, p.Tyr205Ter) manifested connective tissue abnormalities, including tall stature, hernia, hypermobile joints, thin translucent skin, and importantly high myopia (Driver et al., 2020). These clinical findings highlight a role for *EFEMP1* in ocular development, however how *efemp1* is involved in ocular refractive development remains largely unknown.

In the current study, using a zebrafish model with retina-specific *efemp1* modification, we show robust evidence that *efemp1* regulates ocular growth in a light-dependent manner in zebrafish. In particular, mutant fish developed myopia and enlarged eyes when reared under normal lighting, but became emmetropic after dark-rearing (a myopia-inducing condition for normal fish). In addition, we show that *efemp1* may mediate ocular growth by regulating expression of *early growth response 1* (*egr1*), *transforming growth factor beta 1b* (*tgfb1a*), *vascular endothelial growth factor Ab* (*vegfab*) and *retinol binding protein 3* (*rbp3*), and modulating light-dependent responses of *Wnt family 2B* (*wnt2b*) and *vegfab*. Meanwhile, retinal *efemp1* modification influences inner retinal distribution of matrix metalloproteinase 2 (MMP2) and tissue inhibitor of metalloproteinase 2 (TIMP2) for both intrinsic and visually induced ocular growth. This study demonstrates the capacity of a comprehensive zebrafish analysis platform, combining genetic and environmental manipulations, as well as multifaceted

86 phenotypic assessments, to gain insights into GWAS-associated myopia-risk genes in myopia
87 development.

88

89 ## Results

90 ### Retina-specific disruption of *efemp1* leads to reduced visual sensitivity

91 In order to investigate the role of the *efemp1* gene and its interaction with visual environment, we first
92 generated a zebrafish line with *efemp1* modification specifically in the retina (*efemp1*$^{2C\text{-}Cas9}$; Fig 1A),
93 the light-sensing tissue in the eye, using a 2C-Cas9 somatic CRISPR gene editing system (Di Donato
94 et al., 2016). In this transgenic zebrafish line, Tg(*rx2*:*Gal4*) is expressed specifically in the retina and
95 the RPE (Chuang and Raymond, 2001), due to the retina-specific *retinal homeobox gene 2* (*rx2*)
96 promoter. The Gal4 transcription factor binds the upstream activating sequence (UAS) element of the
97 2C-Cas9 transgene Tg(*UAS*:*Cas9T2ACre*;*U6*:*efemp1sgRNA1*;*U6*:*efemp1sgRNA2*), leading to
98 expression of the Cas9 nuclease and Cre recombinase. The retina-specific Cas9 nuclease then combines
99 with universally expressed *efemp1* small guide RNAs (sgRNAs), which target exons 3 and 5 of the
100 *efemp1* genome DNA (gDNA) for CRISPR gene editing in the retina (Fig 1B). The Cre recombinase
101 recombines loxP sites in the Tg(*bact2-loxP-mCherry-loxP-eGFP*) and switches mCherry to eGFP
102 fluorophore reporter specifically in the eye, thus allowing for selection of Cas9-positive mutants (Fig
103 1A′). The patchiness of Cas9 expression in the mutant retina may attribute to the Gal4/UAS system
104 (Halpern et al., 2008). This gene editing system led to mosaic retinal mutations; each Cas9-expressing
105 retinal cell that were driven by the *rx2* promoter would perform its own CRISPR gene editing process,
106 and as a result, even in an individual retina, there were different types of indels (e.g., loss- or gain-of-
107 function mutations, milder mutations that may cause mislocalization) in different cells. Despite the
108 mosaicism, the mutations resulted from the 2C-Cas9 system in retinal cells is expected to be sustained.
109 Also, in adult teleost, activation of *rx2* in retinal stem cells in the retinal ciliary marginal zone
110 determines its fate to form retinal neurons (Reinhardt et al., 2015). This suggested that in new neurons
111 derived from retinal stem cells in the adult zebrafish retina, there is expression of *rx2* to drive the 2C-

112 Cas9 system for genetic modification. Genetic control fish (*efemp1*$^{+/+}$) had the same transgenic
113 background except that they lacked the 2C-Cas9 transgene.

114 We used headloop PCR, which specifically suppresses amplification of wildtype (unmutated) DNA
115 sequences containing sgRNA target sites, but allows targeted mutant sequences to undergo normal PCR
116 amplification. We showed that there were discernibly higher amounts of PCR products amplified from
117 30 ng of *efemp1*$^{2C\text{-}Cas9}$ eye gDNA than from 30 ng of control eye gDNA for both target sites,
118 demonstrating that there were mutations in the mutant zebrafish retina (Fig 1C–D). However, the
119 headloop PCR bands of *efemp1*$^{2C\text{-}cas9}$ fish were remarkably weaker than standard PCR bands, suggesting
120 a low mutation rate. This may have arisen as our gDNA was extracted from whole zebrafish eyes rather
121 than just the retina or Cas9+ cells. On the other hand, due to the mosaic nature of the gene editing, the
122 patchiness of Cas9-expressing retinal cells (Fig 1A′) and the potentially low editing rate, as well as the
123 unavailability of commercial anti-EFEMP1 antibodies that targets specifically the CRISPR editing sites,
124 *efemp1* modification in our mutant model at the protein level is challenging to show.

125 Our preliminary data showed that 5 days post-fertilization (dpf) fish with *efemp1* knockdown by
126 morpholino presented reduced spatial-frequency tuning functions (unpublished). Therefore, we tested
127 optomotor responses (OMR) for our mutant fish to verify modification of *efemp1* at the behavioral level.
128 Our 5 dpf *efemp1*$^{2C\text{-}Cas9}$ mutants showed altered spatial-frequency tuning functions ($P = 0.0334$; Fig 1E),
129 with a significant amplitude reduction ($P = 0.0412$; Fig 1F) in *efemp1*$^{2C\text{-}Cas9}$ fish. There was no
130 difference in peak spatial frequency (Fig 1G) and function bandwidth (Fig 1H) between genotypes.
131 OMR assessment at 2 weeks post-fertilization (wpf) returned similar differences between mutants and
132 their wildtype counterparts (spatial-frequency tuning function: $P = 0.0034$; amplitude: $P = 0.0022$; Fig
133 S1). Taken together, *efemp1*$^{2C\text{-}Cas9}$ fish are a robust model of retinal *efemp1* modification.

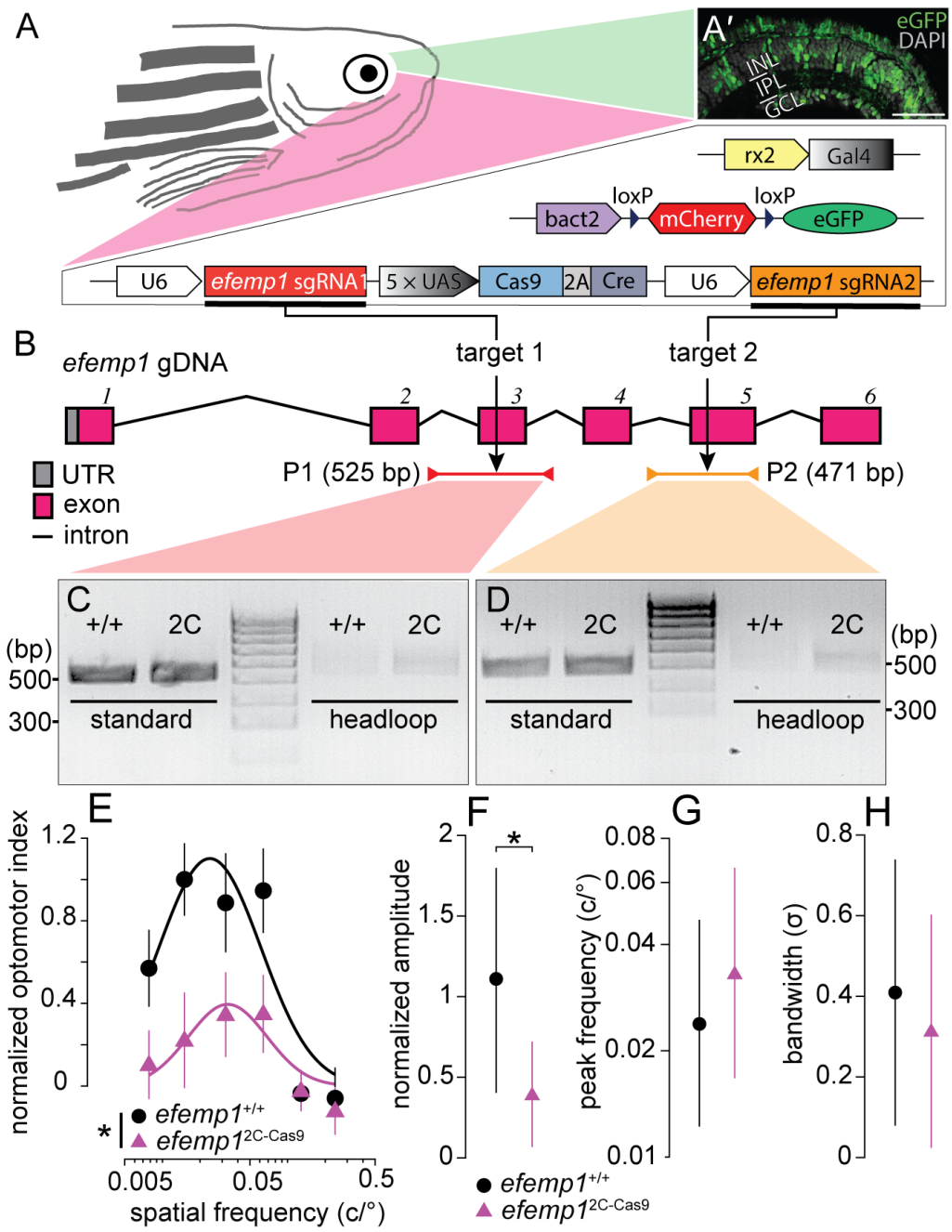

Figure 1. **Genotypic details of retina-specific *efemp1*-modified mutants (*efemp1*$^{2C\text{-}Cas9}$) and phenotypic verification via optomotor responses at 5 days post-fertilization (dpf). (A)** The *efemp1*$^{2C\text{-}Cas9}$ fish were generated using 2C-Cas9 somatic gene editing. Mutant fish have three separate transgenes: Tg(*rx2*:*Gal4*) × Tg(*bact2-loxP-mCherry-loxP-eGFP*) × Tg(*UAS*:*Cas9T2ACre*;*U6*:*efemp1sgRNA1*;*U6*:*efemp1sgRNA2*). Co-expression of these transgenic elements result in expression of green fluorescence (eGFP) in zebrafish retina, indicative of successful Cas9 protein expression. **(A′)** Representative retinal image from a 6 dpf fish. Nuclei stained with DAPI are shown in grey. INL, inner nuclear layer; IPL, inner plexiform layer; GCL, ganglion cell layer. Scale bar: 40 µm. **(B)** The universally expressed *efemp1* sgRNA1 and sgRNA2 from the transgene binds with Cas9 nucleases and cuts exons 3 and 5 of the *efemp1* genome DNA (gDNA), respectively. Standard PCR primers used for genotyping the target sites 1 and 2 amplified 525- (Product 1, P1; spinning from the introns before to after the exon 3) and 471-base pairs (bp; P2; spinning from the intron before to the end of exon 5) of DNA sequences, respectively. Products of headloop PCR are 23-bp longer for P1 and 20-bp longer for P2 due to the headloop tags in reverse primers. UTR, untranslated region. **(C–D)** Gel electrophoresis of the products from standard and headloop PCR for genotyping targeted sites 1 **(C)** and 2 **(D)**. In both images, the middle lanes show a 100-bp reference ladder; positions of 300 and 500 bp of size are indicated for both gel images. **(E–H)** Results of optomotor responses. Spatial-frequency tuning functions **(E)** for 5 dpf *efemp1*$^{+/+}$ (n = 14) and *efemp1*$^{2C\text{-}Cas9}$ fish (n = 13) are three-parameter log-Gaussian functions fit to the data by minimizing the least-square error. The fitted parameters, including **(F)** normalized amplitude, **(G)** peak frequency and **(H)** bandwidth, were compared between groups **Group data are shown** as mean ± SEM in (E) and mean with 95% confidence intervals in (F–H). *$P < 0.05$ (*F*-test).

152 **Disruption of *efemp1* causes myopia and abnormal ocular development in zebrafish**

153 We investigated the development of ocular refraction in *efemp1*$^{2C\text{-}Cas9}$ mutant zebrafish using optical
154 coherence tomography (OCT) to non-invasively obtain cross-section images of zebrafish eyes. This
155 allowed us to quantify ocular refraction as the ratio of retinal radius to lens radius (R/L ratio; Fig 2A),
156 namely *Matthiessen's Ratio*, which is a common means to return axial ocular refraction for aquatic
157 species (Collery et al., 2014; Shand et al., 1999; Turnbull et al., 2015). A higher R/L ratio compared to
158 control fish indicates relative axial myopia, while a lower ratio represents a relative hyperopic shift.
159 Overall, *efemp1*$^{2C\text{-}Cas9}$ fish have higher R/L ratio than *efemp1*$^{+/+}$ fish ($P = 0.0002$), indicating relative
160 myopic ocular structure. *Post-hoc* analysis identified significant relative axial myopia at 2, 6 and 8
161 weeks of age ($P = 0.018$, 0.0001 and 0.002, respectively; Fig 2B).

162 We considered why axial myopia was not significant at 4 wpf in *efemp1*$^{2C\text{-}Cas9}$ fish. EGFP fluorescence
163 levels in the eye appeared to vary between *efemp1*$^{2C\text{-}Cas9}$ fish. We speculated that *efemp1*$^{2C\text{-}Cas9}$ fish with
164 higher eGFP expression indicating higher Cas9 nuclease expression and thus higher rate of CRISPR
165 gene editing, would have more severe visual impairment. As visual impairment can impact feeding, we
166 examined survival rate in low (eGFP+) and high eGFP (eGFP+++) expressing *efemp1*$^{2C\text{-}Cas9}$ fish,
167 differences that were easily distinguished via *post-hoc* histology (Fig 2C). Those *efemp1*$^{2C\text{-}Cas9}$ fish with
168 weaker retinal eGFP expression had higher survival rates than GFP+++ group ($P < 0.0001$; Fig 2C).
169 About 10% of GFP+ fish were lost by 2 wpf ($P = 0.020$) but survival was stable thereafter. In contrast,
170 GFP+++ fish had significantly lower survival rates than GFP+ group at 2 and 4 wpf ($P = 0.0007$ and P
171 < 0.0001, respectively). The survival rate stabilized in GFP+++ from 4 wpf. We interpret these data to
172 indicate that at 4 wpf, loss of the more myopic fish may have contributed to the absence of a significant
173 effect at this age (Fig 2C).

174 We also found that at 5–8 months of age, 7.11% of *efemp1*$^{2C\text{-}Cas9}$ fish appear to have monocular or
175 binocular enlargement (154 fish in total from 5 tanks; Table S1; Fig 2F–I, yellow arrows), compared to
176 *efemp1*$^{+/+}$ fish (Fig 1D–E). In some cases, there was a dark crescent between the eye socket and the
177 ventral eyeball (Fig 2H, white dashed area). Dissection of this eye showed aggressive posterior eye
178 expansion and a scleral crack (Fig 2H insert). Further study is required to confirm whether these rare,

severe scleral cracks represented a greater or faster ocular expansion caused by our retinal *efemp1* modification. Overall, the above results suggest that disruption of *efemp1*$^{2C\text{-}Cas9}$ leads to myopic vision, eye enlargement, and possibly more severe ocular pathology.

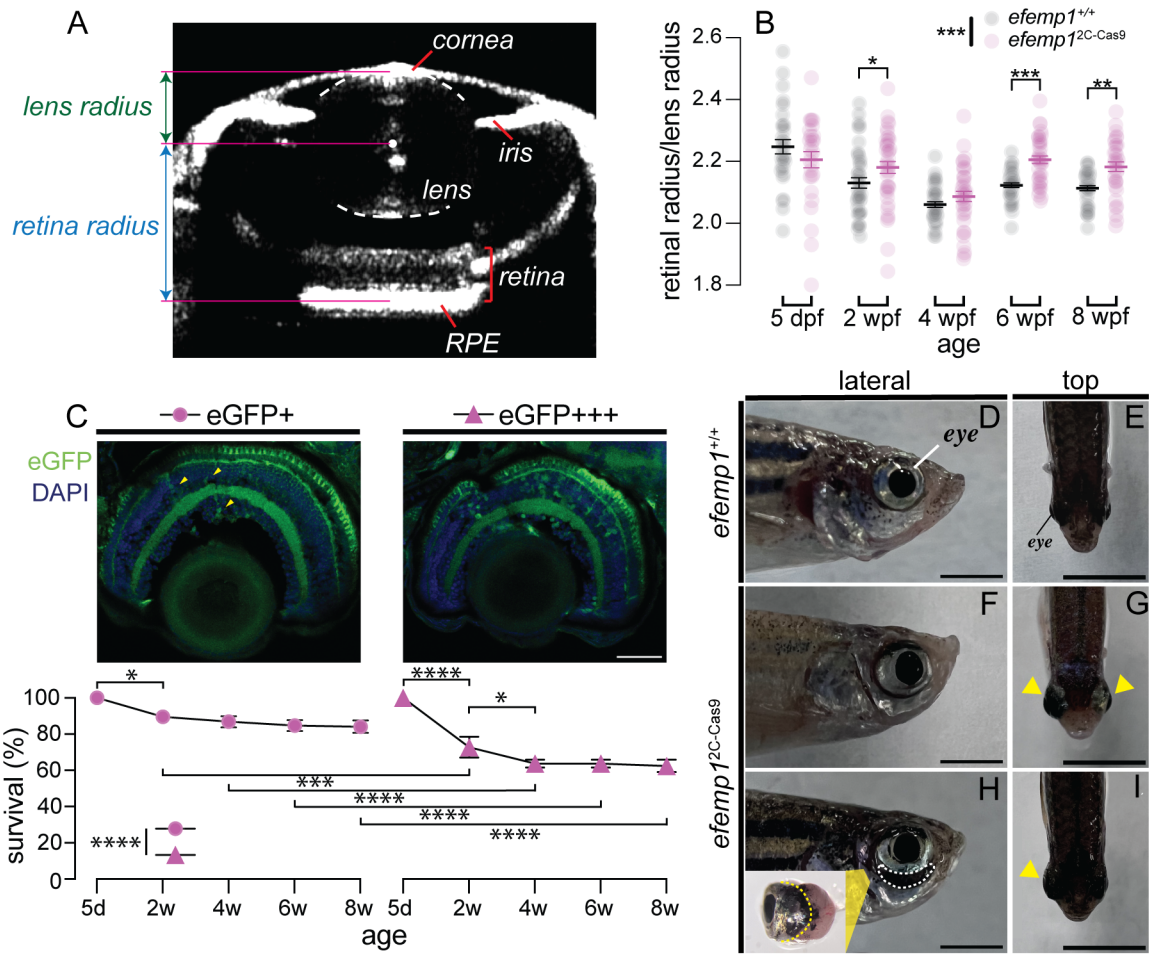

Figure 2. **Ocular development of *efemp1*$^{2C\text{-}Cas9}$ fish under normal rearing.** (A) Representative optical coherence tomography (OCT) image showing eye components, including the cornea, iris, lens, retina and retinal pigment epithelium (RPE). Relative ocular refraction was calculated as the ratio of retinal radius to lens radius. **(B)** Ocular refraction of *efemp1*$^{+/+}$ and *efemp1*$^{2C\text{-}Cas9}$ fish at 5 days post-fertilization (dpf; n = 30 and 29 eyes, respectively), and 2 (n = 40 per genotype), 4 (n = 40 and 38 eyes, respectively), 6 (n = 39 and 40 eyes, respectively), and 8 weeks post-fertilizations (wpf; n = 40 and 34 eyes, respectively)**. Group data are shown as mean ± SEM. (C)** *Efemp1*$^{2C\text{-}Cas9}$ fish were categorized into two groups based on their retinal eGFP levels (eGFP+ vs. eGFP+++). Sporadic eGFP positive cells (highlighted by yellow arrows) are evident in the eGFP+ retinal image, whereas the eGFP+++ retinal image had more EGFP cells. Scale bar: 40 µm. Survival rates for eGFP+ and eGFP+++ groups from 5 days (d; set as 100%) to 8 weeks (w) of age are presented as mean ± SEM. Three tanks per group were analyzed. **P < 0.05*; ***P < 0.01*; *****P < 0.0001*. *Two*-way ANOVA and Fisher's LSD *post-hoc* tests were performed. In **(C)**, for comparisons within each eGFP level, only significant survival differences between a time point and its adjacent time are shown. **(D–I)** Representative images of eye morphology for *efemp1*$^{+/+}$ **(D–E)** and *efemp1*$^{2C\text{-}Cas9}$ fish **(F–I)** reared under normal lighting at 1 year old. Yellow arrowheads indicate enlarged eyes. Dashed region below the eye in **(H)** highlights a scleral crack shown in the zoom-in image insert, in which the yellow dashed line indicates the estimated normal position of the posterior eye of zebrafish. Scale bars: 3 mm.

199 **EFEMP1 deficits in the retina results in altered retinal function**

200 The retina plays a crucial role in the local regulation of eye growth, a process that does not require input
201 from the brain (Troilo et al., 1987; Wallman et al., 1987). To examine whether retinal function is
202 involved in the abnormal development of ocular refraction in the *efemp1*$^{2C\text{-}Cas9}$ fish, electroretinograms
203 (ERG) were recorded at 2, 4, 6 and 8 wpf.

204 At 2 weeks of age, *efemp1*$^{2C\text{-}Cas9}$ fish showed significantly lower photoreceptoral *a*-wave amplitude (P
205 $= 0.0118$), especially at higher stimulus intensities (Fig 3A$_2$), compared to *efemp1*$^{+/+}$ fish. However, *b*-
206 wave amplitude was similar between mutants and control fish (Fig 3A$_1$). *A*- and *b*-wave implicit times
207 of *efemp1*$^{2C\text{-}Cas9}$ fish were significantly faster than that of *efemp1*$^{+/+}$ fish ($P = 0.018$ and 0.0047,
208 respectively; Fig 3A, 4A$_3$–A$_4$).

209 At 4 wpf (Fig 3B–B$_4$), *efemp1*$^{2C\text{-}Cas9}$ fish showed smaller *b*-wave amplitude ($P < 0.0001$; Fig 3B$_1$), but
210 no difference in *a*-wave amplitude (Fig 3B$_2$) compared with *efemp1*$^{+/+}$ fish. *Two*-way ANOVA also
211 indicated significantly slower *b*-wave ($P = 0.0052$, Fig 3B$_3$) and *a*-wave ($P < 0.0001$, Fig 3B$_4$) in
212 *efemp1*$^{2C\text{-}Cas9}$ fish.

213 At 6 wpf, both *a*- and *b*-wave amplitudes were significantly smaller in *efemp1*$^{2C\text{-}Cas9}$ relative to *efemp1*$^{+/+}$
214 fish (effects of genotypes: $P < 0.0001$ for both *a*- and *b*-wave; Fig 3C–C$_2$). *Efemp1*$^{2C\text{-}Cas9}$ fish had
215 significantly slower *b*-wave (effect of genotypes: $P = 0.0182$, Fig 3C$_3$) and *a*-wave responses ($P =$
216 0.0068 for –2.11 log cd.s.m^{-2}; Fig 3C$_4$) than *efemp1*$^{+/+}$ fish.

217 At 8 wpf (Fig 3D), both *b*-wave ($P = 0.012$; Fig 3D$_1$) and *a*-wave amplitudes ($P < 0.0001$; Fig 3D$_2$)
218 were a little larger in *efemp1*$^{2C\text{-}Cas9}$ compared to *efemp1*$^{+/+}$ fish. A clear effect of genotypes was evident
219 in terms of slower *b*-waves ($P = 0.0012$; Fig 3D$_3$) and *a*-waves ($P = 0.015$; Fig 3D$_4$) in *efemp1*$^{2C\text{-}Cas9}$
220 fish. A longer latency before initiation of the *b*-wave might expose a larger proportion of the electro-
221 negative photoreceptoral *a-wave* responses, accounting for the observed larger but slower *a-waves*.

222 Although it is unclear why *efemp1*$^{2C\text{-}Cas9}$ mutants show faster response at a young age, but slower
223 response at 4-8 wpf, it is apparent that retinal dysfunction is a robust phenotype of this genetic myopia
224 mutant model.

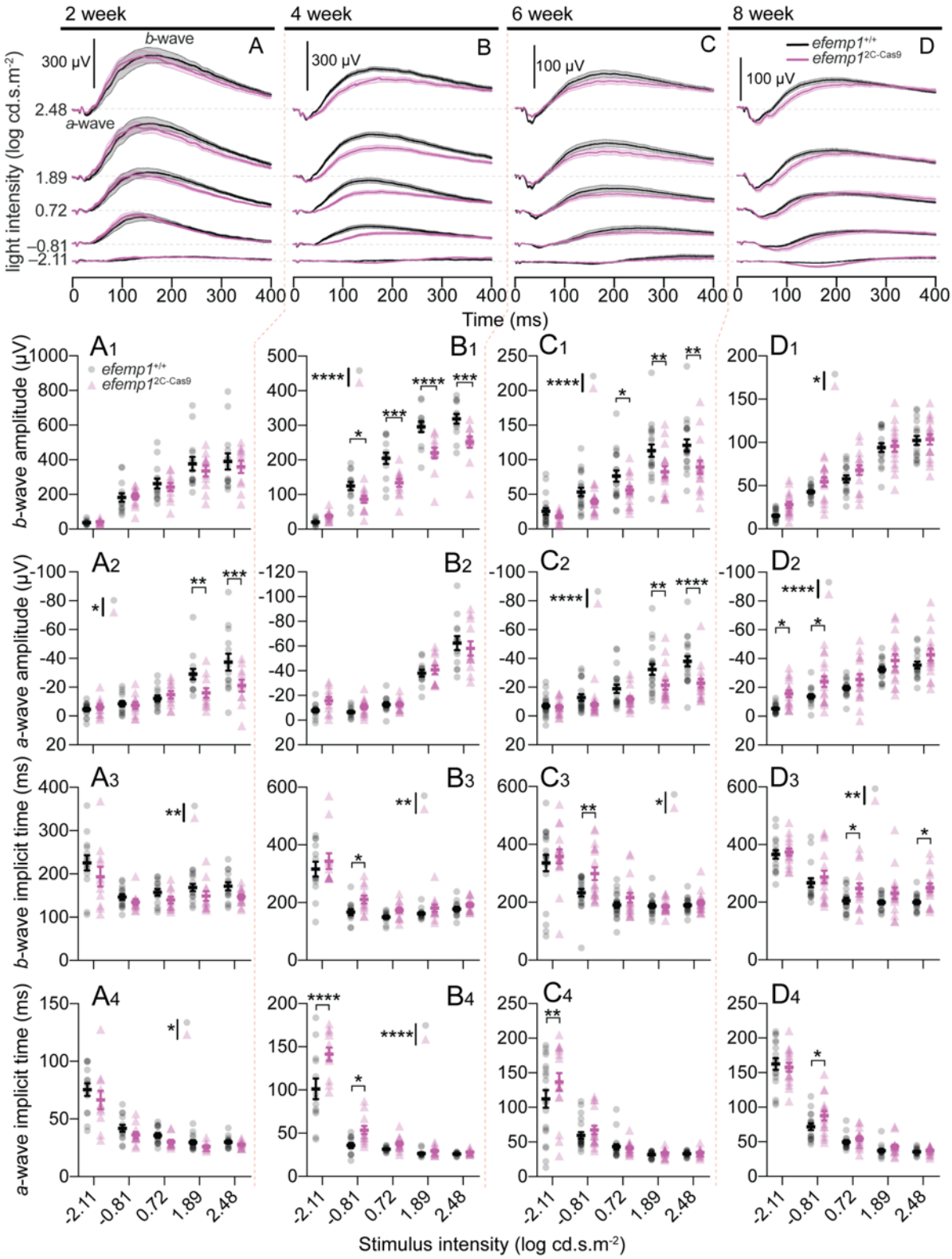

Figure 3. **Electroretinogram (ERG) results of *efemp1*$^{+/+}$ and *efemp1*$^{2C\text{-}Cas9}$ fish under normal rearing. (A, B, C, D)** Group average ERG traces with shades areas indicating SEM, **(A_1, B_1, C_1, D_1)** *b*-wave amplitudes, **(A_2, B_2, C_2, D_2)** *a*-wave amplitudes, **(A_3, B_3, C_3, D_3)** *b*-wave implicit times and **(A_4, B_4, C_4, D_4)** *a*-wave implicit times at 2 **(A–A_4, respectively)**, 4 **(B–B_4, respectively)**, 6 **(C–C_4, respectively)** and 8 **(D–D_4, respectively)** weeks post-fertilization (wpf). There were 14 and 11 eyes for 2 wpf, 13 and 12 eyes for 4 wpf, 20 and 17 eyes for 6 wpf, and 17 and 16 eyes for 8 wpf *efemp1*$^{+/+}$ and *efemp1*$^{2C\text{-}Cas9}$ fish, respectively. Scale bars: 300 µV in **(A–B)** and 100 µV in **(C–D)**. Group data are shown as mean ± SEM. *T*wo-way ANOVA and Fisher's LSD *post-hoc* tests were performed. **P < 0.05*; ***P< 0.01*; ****P < 0.001*; *****P < 0.0001*.

233 **Zebrafish with retinal *efemp1* disruption become emmetropic after dark-rearing**

234 As our results showed that *efemp1* disruption led to myopia development in zebrafish under normal
235 lighting, we further investigated whether *efemp1* modification might exacerbate the myopia-inducing
236 effects of dark-rearing (Fig 4A) (Xie et al., 2023 Preprint).

237 After 2 weeks of rearing under normal lighting, *efemp1*$^{2C\text{-}Cas9}$ fish had developed myopia compared with
238 *efemp1*$^{+/+}$ fish ($P < 0.0001$). Interestingly, after 2 weeks of dark-rearing, *efemp1*$^{2C\text{-}Cas9}$ fish did not
239 undergo a myopic shift ($P < 0.0001$, Fig 4B), and had similar ocular fraction to *efemp1*$^{+/+}$ fish reared
240 under normal light.

241 After 4 weeks of dark-rearing, control *efemp1*$^{+/+}$ fish became myopic ($P = 0.025$; Fig 4B). However,
242 similar to 2-week results, relative to normal-light-reared *efemp1*$^{+/+}$ fish, *efemp1*$^{2C\text{-}Cas9}$ fish were myopic
243 when reared under normal lighting ($P < 0.0001$), but after dark-rearing they maintained a R/L ratio that
244 was consistent with emmetropic vision at this age (Fig 4B).

245 A *three*-way ANOVA reveals a significant interaction between genotypes and environmental conditions
246 ($P < 0.0001$). These results indicated that under normal visual conditions *efemp1* is needed for
247 emmetropization, however under aberrant visual conditions the lack of *efemp1* can interfere with
248 mechanisms that usually drive myopia development.

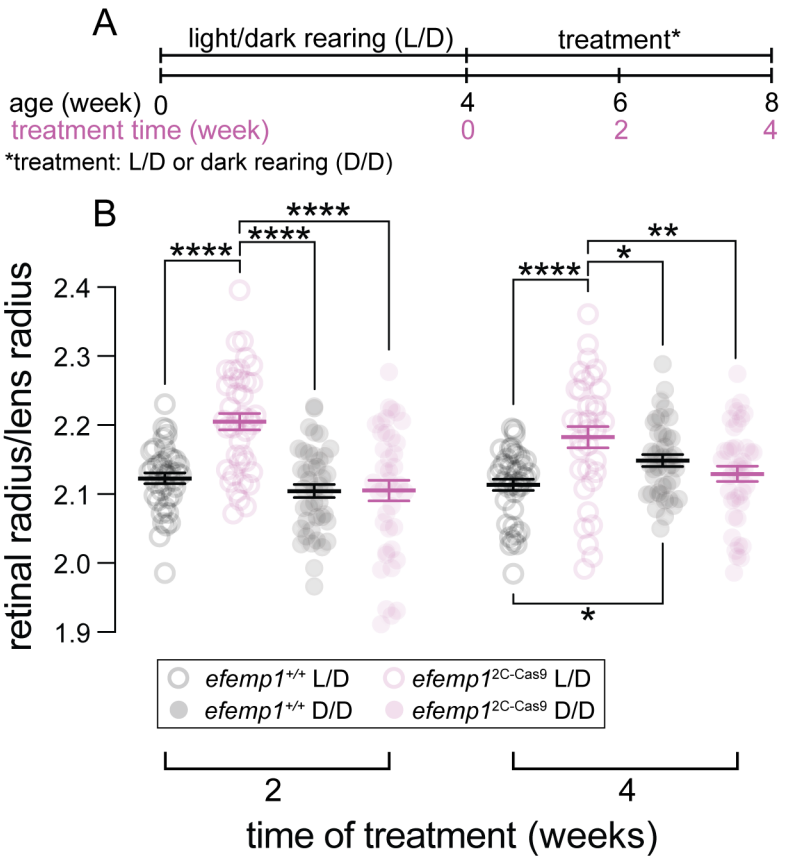

Figure 4. **Ocular refraction of *efemp1*$^{+/+}$ and *efemp1*$^{2C\text{-}Cas9}$ fish after environmental treatment. (A)** *Efemp1*$^{+/+}$ and *efemp1*$^{2C\text{-}Cas9}$ fish were reared under normal light/dark cycle (L/D) until 4 weeks post-fertilization (wpf) and either continued under normal lighting (L/D) or switched to dark-rearing (D/D) for 2 or 4 weeks (to 6 or 8 wpf, respectively). **(B)** Relative ocular refraction of L/D- or D/D-reared *efemp1*$^{+/+}$ and *efemp1*$^{2C\text{-}Cas9}$ eyes were quantified after 2 or 4 weeks of treatment using optical coherence tomography (OCT). There were 39, 40, 42 and 40 eyes at the 2-week time point, and 40, 34, 40 and 40 eyes at the 4-week time point for L/D-reared *efemp1*$^{+/+}$, L/D-reared *efemp1*$^{2C\text{-}Cas9}$, D/D-reared *efemp1*$^{+/+}$, D/D-reared *efemp1*$^{2C\text{-}Cas9}$ fish, respectively. Group data are shown as mean ± SEM. *Three*-way ANOVA and Fisher's LSD *post-hoc* analyses were performed. *$P < 0.05$; **$P < 0.01$; ***$P < 0.001$; ****$P < 0.0001$.

Retinal *efemp1* modification drives retinal physiological changes in response to dark-rearing

To investigate whether *efemp1* is involved in dark-rearing-induced retinal functional changes, we analyzed ERG of *efemp1*$^{+/+}$ and *efemp1*$^{2C\text{-}Cas9}$ fish after 2 days, 2 or 4 weeks of normal light or dark-rearing.

After 2 days of treatment, under either rearing condition, *efemp1*$^{2C\text{-}Cas9}$ fish showed smaller ERG responses than *efemp1*$^{+/+}$ fish (Fig 5A–D). *Three*-way ANOVA confirmed a significant genotype effect with smaller *b*- and *a*-wave amplitudes, as well as slowed *b*- and *a*-wave implicit times ($P < 0.0001$, $P = 0.0002$, $P = 0.0023$ and $P = 0.021$, respectively; Fig 5E–H) for *efemp1*$^{2C\text{-}Cas9}$ fish. There was a

267 significant interaction between genotypes and rearing conditions for *b*-wave implicit time (*P = 0.0362*;
268 Fig 5G).

269 Functional outcomes after 2-weeks treatment (Fig 5I–L) were similar to those for 2 days of treatment.
270 In general *b*- and *a*-wave amplitudes (*P < 0.0001* for both; Fig 5M–N) were smaller in *efemp1*$^{2C\text{-}Cas9}$
271 fish. After dark-rearing, *efemp1*$^{2C\text{-}Cas9}$, but not *efemp1*$^{+/+}$ fish showed further *b*-wave reduction (*P =*
272 *0.031* at 1.87 log cd.s.m^{-2}; Fig 5M). *Three*-way ANOVA returned significant interactions between
273 genotype and dark-rearing on *a*-wave amplitude (*P = 0.0396*), with *efemp1* disruption further
274 attenuating dark-rearing-induced photoreceptor responses (Fig 5N). In particular, after dark-rearing, *a*-
275 wave amplitudes were smaller at all tested intensities for *efemp1*$^{+/+}$ fish (*P = 0.042*, *P = 0.0004* and *P <*
276 *0.0001* for –0.83, 0.73 and 1.87 log cd.s.m^{-2}, respectively), but only at the highest intensity for *efemp1*$^{2C\text{-}}$
277 ^{Cas9} fish (*P = 0.0009*; Fig 5N). We did not find difference in *b*-wave implicit time between groups (Fig
278 5O), however both *efemp1*$^{+/+}$ and *efemp1*$^{2C\text{-}Cas9}$ fish had slower *a*-wave implicit time after dark-rearing
279 at –0.83 log cd.s.m^{-2} (*P = 0.012* and *0.010*, respectively; Fig 5P). Overall, these results suggested that
280 *efemp1* modification exacerbates functional changes seen with dark-rearing.

281 At the 4-week time point, under either rearing condition *efemp1*$^{2C\text{-}Cas9}$ fish had smaller and slower *b*-
282 waves than *efemp1*$^{+/+}$ fish (*P < 0.0001* and *P = 0.002*, respectively; Fig 5Q–T, 5U and 5W,). *A*-waves
283 in mutants were slightly larger and slower (Fig 5V and 5X, *P < 0.0001*). The waveform indicates that
284 slower *b*-waves expose more of the photoreceptoral response, making the *a*-wave both larger and slower.

285 Taken together, at 2 dpf and 2 wpf, significant statistical interactions indicate that *efemp1* modification
286 affects the way that dark-rearing impacts retinal physiology.

287

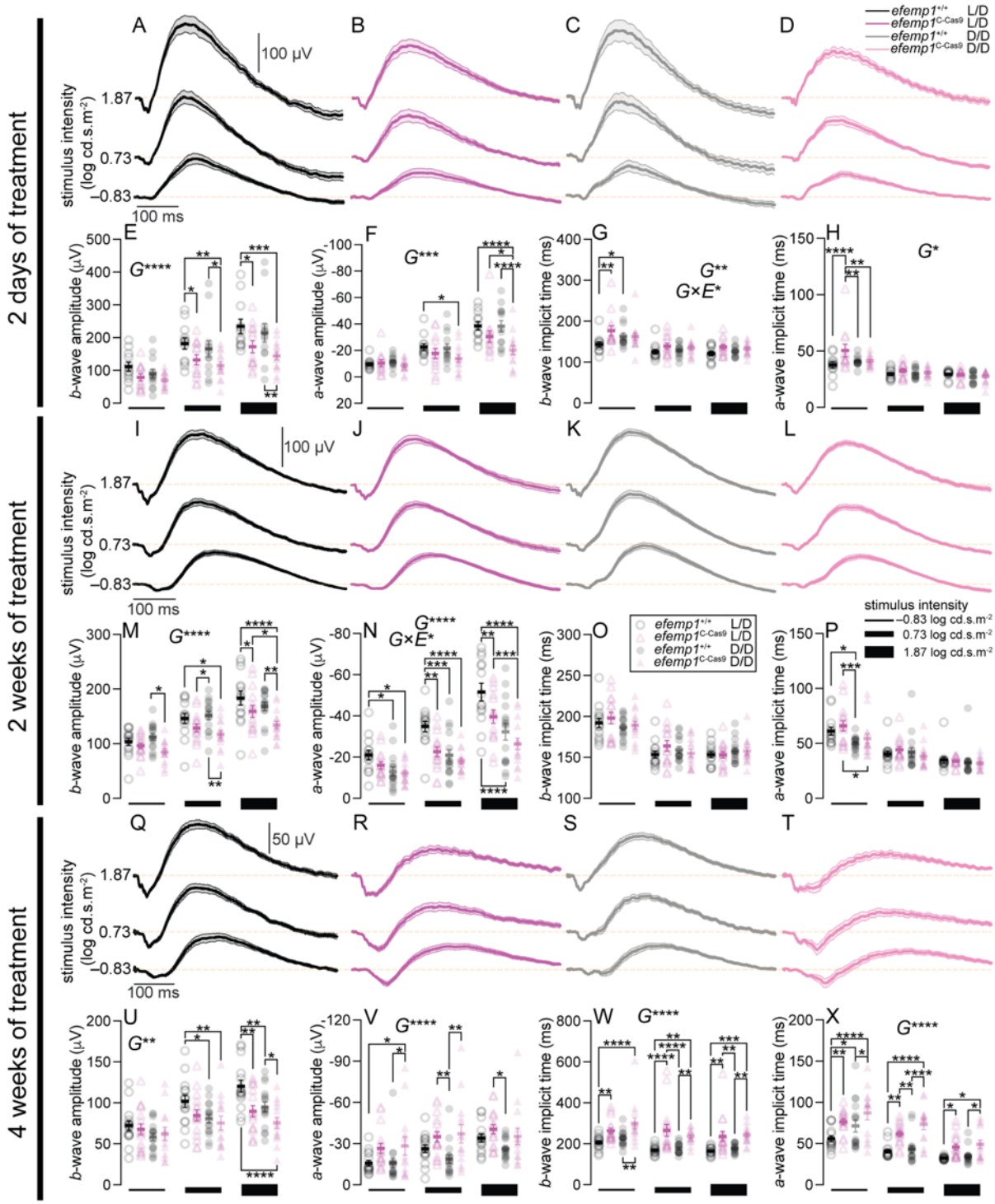

Figure 5. **Electroretinography (ERG) of *efemp1*$^{+/+}$ and *efemp1*$^{2C\text{-}Cas9}$ fish after 2 days, 2 weeks or 4 weeks of light/dark-cycle (L/D) or dark (D/D) rearing.** **(A–H)** Group average ERG traces for **(A)** L/D-reared *efemp1*$^{+/+}$ (n = 12), **(B)** L/D-reared *efemp1*$^{2C\text{-}Cas9}$ (n = 13), **(C)** D/D-reared *efemp1*$^{+/+}$ (n = 13) and **(D)** D/D-reared *efemp1*$^{2C\text{-}Cas9}$ eyes (n = 14). Shaded areas indicated SEM. Group **(E)** *b*-wave amplitude, **(F)** *a*-wave amplitude, **(G)** *b*-wave implicit time and **(H)** *a*-wave implicit times measured after 2 days of treatment. Vertical scale bar indicates 100 µV and horizontal scale bar represents 100 ms in **(A–D)**. **(I–P)** Group average ERG traces for **(I)** L/D-reared *efemp1*$^{+/+}$ (n = 14), **(J)** L/D-reared *efemp1*$^{2C\text{-}Cas9}$ (n = 15), **(K)** D/D-reared *efemp1*$^{+/+}$ (n = 16) and **(L)** D/D-reared *efemp1*$^{2C\text{-}Cas9}$ eyes (n = 15), as well as their **(M)** *b*-wave amplitude, **(N)** *a*-wave amplitude, **(O)** *b*-wave implicit time and **(P)** *a*-wave implicit time measured after 2 weeks of treatment. **(Q–X)** Group average ERG traces for **(Q)** L/D-reared *efemp1*$^{+/+}$ (n = 15), **(R)** L/D-reared *efemp1*$^{2C\text{-}Cas9}$ (n = 16), **(S)** D/D-reared *efemp1*$^{+/+}$ (n = 16) and **(T)** D/D-reared *efemp1*$^{2C\text{-}Cas9}$ eyes (n = 14), as well as their **(U)** *b*-wave amplitude, **(V)** *a*-wave amplitude, **(W)** *b*-wave implicit time and **(X)** *a*-wave implicit time measured after 4 weeks of treatment. Group data are shown as mean ±SEM. ERGs were measured at –0.83, 0.73 and 1.87 log cd.s.m^{-2} of stimulus intensities, represented by black blocks of different sizes below

301 graphs; thicker blocks indicate higher intensities. *Three*-way ANOVA and Fisher's LSD *post-hoc* tests were performed.
302 Significant main effects of genotypes (*G*) and interactions between genotypes and rearing conditions (*G*×*E*) are indicated in
303 the graphs. *$P < 0.05$; **$P < 0.01$; ***$P < 0.001$; ****$P < 0.0001$.
304

305 **Retinal *efemp1* modification changes expression of myopia-associated genes under normal rearing**
306 **and their responses to dark-rearing**

307 In order to investigate potential molecular pathways through which retinal *efemp1* modification impacts
308 refractive development under normal and dark-rearing, we quantified expression of a group of known
309 myopia-associated genes using RT-qPCR after 2 days and 4 weeks of environmental manipulation.
310 These timepoints broadly align with initiation (2 days) and consolidation (4 weeks) phases of myopia
311 development in zebrafish (Fig 6A).

312 We first quantified the expression of *efemp1* and found lower *efemp1* expression in *efemp1*$^{2C\text{-}Cas9}$ than
313 in *efemp1*$^{+/+}$ fish under normal and dark-rearing ($P = 0.0248$ and 0.0295, respectively) but only at the
314 later time point (Fig 6B).

315 The *early growth response 1* (*egr1*) gene is an immediate early response transcriptional factor that has
316 been shown to be up-regulated when the eye is exposed to hyperopia-inducing or myopia-suppressing
317 visual environments, and down-regulated when the eye is under myopia-inducing visual conditions
318 (Ashby et al., 2014; Fischer et al., 1999). Loss of this gene promotes myopia in mice (Schippert et al.,
319 2007). In our data, there were genotype ($P = 0.042$) and dark-rearing effects ($P < 0.0001$) on *egr1*
320 expression. After 2 days of normal light rearing, *egr1* expression was up-regulated in *efemp1*$^{2C\text{-}Cas9}$ fish
321 compared to *efemp1*$^{+/+}$ fish (~ 4 wpf; $P = 0.0002$). *Egr1* expression was then down-regulated later after
322 4 weeks in normal lighting (8 wpf; $P = 0.018$). After 2 days of dark-rearing, both genotypes showed
323 reduced *egr1* expression ($P < 0.0001$ for both). After 4 weeks of dark-rearing, only *efemp1*$^{+/+}$ fish
324 showed down-regulated *egr1* expression ($P = 0.0011$) and no further change was seen in *efemp1*$^{2C\text{-}Cas9}$
325 fish (Fig 6C).

326 *Transforming growth factor beta* genes (*tgfbs)* encode fundamental secreted TGF-βs, which has been
327 shown to be down-regulated in form-deprived myopic tree shrew eyes to impact collagen synthesis
328 (Jobling et al., 2004) and in particular matrix metalloproteinase 2 (MMP2) (Itoh et al., 2010). Our results

329 showed that expression of *tgfb1a* was impacted by genotype and rearing condition ($P = 0.0292$ and
330 0.0070, respectively). At the 4-week timepoint, under either normal or dark-rearing, *efemp1*$^{2C\text{-}Cas9}$ fish
331 showed lower *tgfb1a* expression than *efemp1*$^{+/+}$ fish ($P = 0.0038$ and 0.0205, respectively). *Tgfb1a*
332 expression was reduced in both *efemp1*$^{+/+}$ and *efemp1*$^{2C\text{-}Cas9}$ fish after dark-rearing ($P = 0.0051$ and
333 0.0271, respectively; Fig 6D). The expression of *tgfb1b* was primarily influenced by dark-rearing ($P =$
334 0.0047); both *efemp1*$^{+/+}$ and *efemp1*$^{2C\text{-}Cas9}$ fish showed a reduction after 4 weeks of dark-rearing ($P =$
335 0.0003 and 0.0041, respectively; Fig 6E).

336 The *vascular endothelial growth factor A* (*vegfa*) gene encodes the glycoprotein VEGFA, which
337 contributes to vasculature development, neuronal function (Mackenzie and Ruhrberg, 2012) and
338 extracellular matrix regulation (Kuiper et al., 2007). Decreased retinal VEGFA concentration was found
339 in marmosets with lens-induced myopia (Zhu et al., 2021). For the two zebrafish *vegfa* paralogues,
340 *three*-way ANOVA showed an effect of dark-rearing on expression of both *vegfaa* and *vegfab* ($P <$
341 0.0001 for both). Both *efemp1*$^{+/+}$ and *efemp1*$^{2C\text{-}Cas9}$ fish showed decreased *vegfaa* expression after 2 days
342 ($P = 0.0094$ and 0.0026, respectively) and 4 weeks of dark-rearing ($P = 0.0002$ and 0.012, respectively;
343 Fig 6F). *Vegfab* down-regulation was found in both *efemp1*$^{+/+}$ and *efemp1*$^{2C\text{-}Cas9}$ fish after 2 days of dark-
344 rearing ($P < 0.0001$ and $P = 0.0007$, respectively) but was only observed in *efemp1*$^{+/+}$ fish at week 4 (P
345 $= 0.0001$). A significant interaction between genotypes and rearing conditions shown by *three*-way
346 ANOVA analysis ($P = 0.0125$), is indicative of a smaller dark-rearing-induced reduction in *vegfab*
347 expression due to *efemp1* disruption. Indeed, retinal *efemp1* disruption *per se* had led to a down-
348 regulation of *vegfab* under normal rearing ($P = 0.039$ and 0.035 at the 2-day and 4-week time points,
349 respectively; Fig 6G).

350 Insulin-like growth factor 1 (IGF1), an endocrine growth hormone, is produced in the liver and then
351 delivered to other organs, playing an important role in overall growth during development
352 (Stratikopoulos et al., 2008). A previous study reported that *igf1* was up-regulated in form-deprived
353 myopic guinea pigs (Ding et al., 2020). However, we did not observed difference in *igf1* expression
354 between groups in our experiments (Fig 6H).

355 Fibroblast growth factor (FGF2) has functions in embryonic development, angiogenesis, wound healing,
356 cell differentiation and neuronal function (e.g., photoreceptor transduction) (Bikfalvi et al., 1997). With
357 form-deprivation myopia, *fgf2* expression was reported to be down-regulated in the chick sclera but up-
358 regulated in guinea pig retinae (An et al., 2012; Seko et al., 1995). Our *three*-way ANOVA analysis
359 showed an effect of rearing conditions on *fgf2* expression ($P = 0.0432$). Only *efemp1*$^{+/+}$ but not *efemp1*$^{2C-}$
360 ^{Cas9} fish showed a reduction of *fgf2* expression after 2 days of dark-rearing ($P = 0.0392$), suggesting that
361 *efemp1* disruption may attenuate dark-rearing induced changes in *fgf2* expression (Fig 6I). Yet, our data
362 showed no statistical significance for a gene-environment interaction.

363 The *Wnt family 2B* (*wnt2b*) gene activates the Wnt/β-catenin signaling pathway which is crucial for
364 ocular development (e.g., lens, retinal pigment epithelium, vasculature and rod photoreceptors, etc.)
365 (Blomfield et al., 2023). Mice with form-deprivation myopia were found to show up-regulated *wnt2b*
366 expression (Ma et al., 2014). Our statistics showed a significant interaction between genotype and
367 rearing condition ($P = 0.0096$; Fig 6J). *Efemp1*$^{+/+}$ fish, but not *efemp1*$^{2C\text{-}Cas9}$ fish, showed down-
368 regulation of *wnt2b* expression after 2 days of dark-rearing ($P = 0.0003$), implicating reduced dark-
369 rearing-induced changes in *wnt2b* expression with *efemp1* deficiency.

370 The soluble retinol binding protein 3 (RBP3; or IRBP in mammals) is released into the
371 interphotoreceptor matrix from retinal photoreceptors, mediating retinoid trafficking for the visual cycle
372 (Gonzalez-Fernandez and Ghosh, 2008). Lack of *Rbp3* in mice caused excessive eye growth and myopia
373 (Wisard et al., 2011). In both *efemp1*$^{+/+}$ and *efemp1*$^{2C\text{-}Cas9}$ fish, *rbp3* expression was down-regulated after
374 2 days ($P = 0.0007$ and $P < 0.0001$, respectively) and 4 weeks of dark-rearing ($P < 0.0001$ for both; Fig
375 6K). Rearing condition thus made a major effect on expression of *rbp3* ($P < 0.0001$). Retinal *efemp1*
376 modification also resulted in significantly higher *rbp3* expression in *efemp1*$^{2C\text{-}Cas9}$ fish ($P = 0.044$),
377 particularly after 2 days under normal rearing ($P = 0.0144$; Fig 6K).

378 The *gap junction delta 2* (*gjd2*) gene encodes a predominant gap junction protein, connexin36, in the
379 central nervous system, including the retina, forming electrical synapses for rapid neuronal signaling
380 (Bloomfield and Völgyi, 2009). Recent findings showed that depletion of the two zebrafish paralogues,

381 *gjd2a* and *gjd2b*, caused myopia and hyperopia, respectively (Quint et al., 2021). We found no
382 expression changes in *gjd2a* expression between groups (Fig 6L). In contrast, *three*-way ANOVA
383 analysis showed a main effect of rearing conditions on *gjd2b* expression ($P < 0.0001$). Both *efemp1*$^{+/+}$
384 and *efemp1*$^{2C\text{-}Cas9}$ fish showed an up-regulation after 2 days ($P = 0.0261$ and 0.0368, respectively) and
385 4 weeks of dark-rearing ($P < 0.0001$ and $P = 0.0003$, respectively; Fig 6M).

386

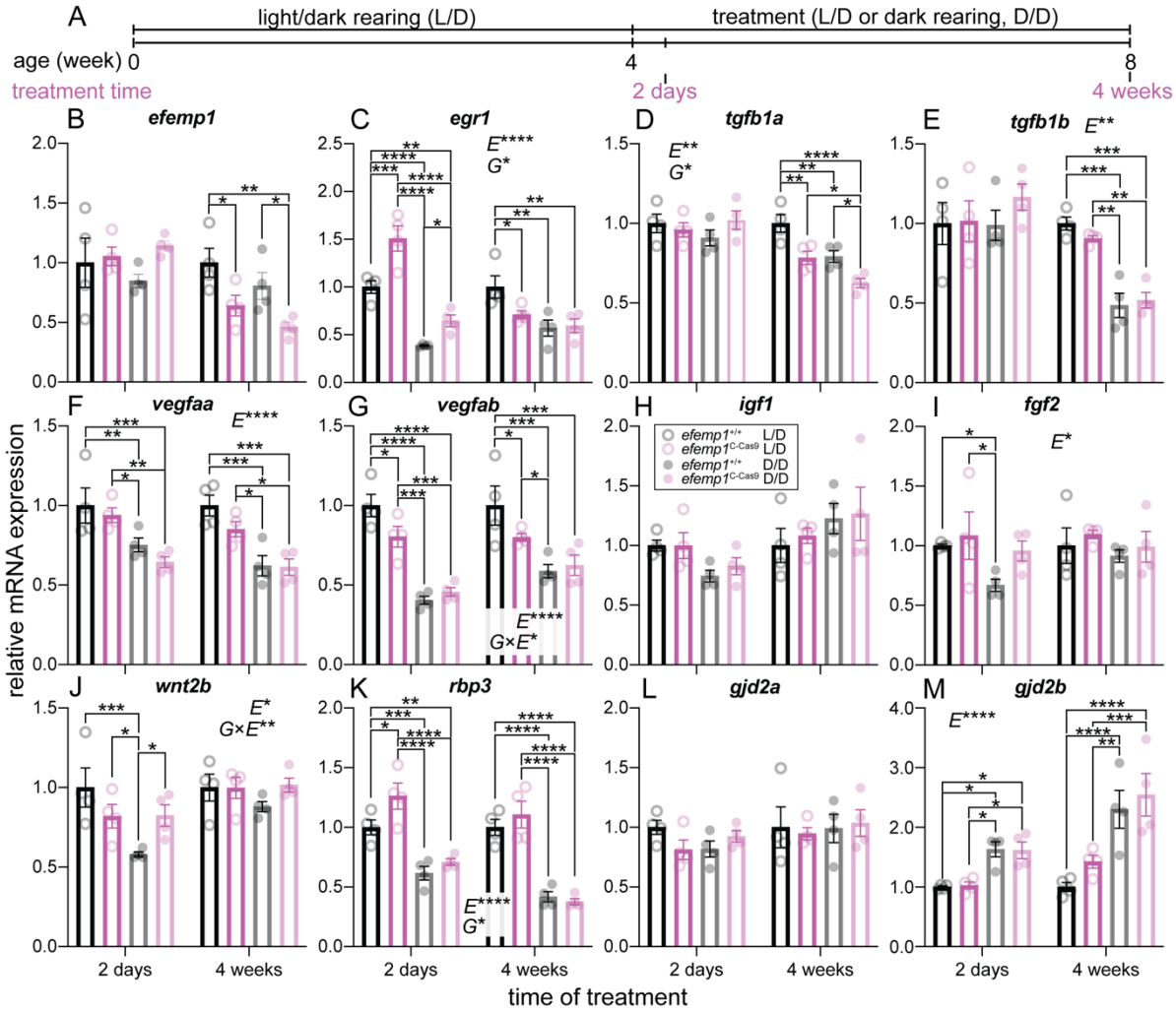

387

388 Figure 6. **Expression of representative myopia-associated genes for *efemp1*$^{+/+}$ and *efemp1*$^{2C\text{-}Cas9}$ fish after 2 days or 4 weeks**
389 **of light/dark-cycle (L/D) or dark (D/D) rearing. (A)** *Efemp1*$^{+/+}$ and *efemp1*$^{2C\text{-}Cas9}$ fish were reared under a standard light/dark-
390 cycle (L/D) to 4 weeks post-fertilization (wpf) and then were reared under L/D or dark tanks (D/D) to up to 8 wpf (4 weeks of
391 treatment). Eyes for molecular analysis were sampled after 2 days or 4 weeks of treatment. Relative mRNA levels of myopia-
392 associated genes, including **(B)** *efemp1*, **(C)** *egr1*, **(D)** *tgfb1a*, **(E)** *tgfb1b*, **(F)** *vegfaa*, **(G)** *vegfab*, **(H)** *igf1*, **(I)** *fgf2*, **(J)** *wnt2b*, **(K)**
393 *rbp3*, **(L)** *gjd2a*, **(M)** *gjd2b* were analyzed for *efemp1*$^{+/+}$ and *efemp1*$^{2C\text{-}Cas9}$ fish after 2 days and 4 weeks of treatment (n = 4
394 samples per group), using qPCR. Group data are shown as mean ± SEM. *Three*-way ANOVA and Fisher's LSD *post-hoc* tests
395 were performed. Significant main effects of genotypes (*G*), rearing conditions (*E*) and their interactions (*G*×*E*) are indicated in
396 the graphs. **P* < 0.05; ***P* < 0.01; ****P* < 0.001; *****P* < 0.0001.

397

398 **Differences in EFEMP1, TIMP2 and MMP2 distributions between *efemp1*$^{+/+}$ and *efemp1*$^{2C\text{-}Cas9}$ fish**
399 **were found after normal and dark-rearing**

400 We examined whether retinal *efemp1* modification affects the distribution of myopia-associated
401 extracellular matrix proteins in the retina after 2 days or 4 weeks of normal or dark-rearing (Fig 7A).

402 With the mosaic pattern of retinal *efemp1* modification (Fig 2C), EFEMP1 protein expression was still
403 evident in the retina (Fig 7B–C). We found that at the 2-day timepoint, *efemp1*$^{2C\text{-}Cas9}$ fish showed a
404 change in EFEMP1 distribution with relatively lower levels in the amacrine cell layer (ACL; effect of
405 genotypes: $P = 0.0079$; Fig 7B$_{1–4}$ and 7B$_{i–ii}$) but higher relative expression in the inner plexiform layer
406 (IPL) compared with *efemp1*$^{+/+}$ fish ($P = 0.0132$; Fig 7B$_{1–2}$ and B$_{i–iii}$). After 2 days of dark-rearing, inner
407 retinal EFEMP1 distribution remained largely unchanged in both genotypes (Fig 7B). At the 4-week
408 timepoint, dark-rearing reduced EFEMP1 expression in the ACL in both genotypes (effect of rearing
409 conditions: $P < 0.0001$; Fig 7C$_{1–4}$ and 7C$_{i–ii}$). A significant interaction was observed for the ganglion
410 cell layer (GCL; $P = 0.0022$; Fig 7C$_{i}$ and C$_{iv}$), with *efemp1*$^{2C\text{-}Cas9}$ fish ($P = 0.0015$), but not *efemp1*$^{+/+}$
411 fish, exhibiting higher relative EFEMP1 expression in the GCL after dark-rearing.

412 Matrix metalloproteinase 2 (MMP2) and tissue inhibitor of metalloproteinase 2 (TIMP2) have long
413 been associated with myopia (Jia et al., 2017; Jia et al., 2014; Liu and Sun, 2018) and our previous data
414 showing that their distribution was changed after dark-rearing (Xie et al., 2023 Preprint).

415 Analyzing their inner retinal distribution, we found that at the 2-day timepoint, relative TIMP2
416 expression in *efemp1*$^{2C\text{-}Cas9}$ fish was overall lower in the ACL but higher in the IPL, compared to control
417 *efemp1*$^{+/+}$ fish (effect of genotypes: $P = 0.0001$ and $P < 0.0001$, respectively; Fig 7D$_{1–4}$ and 7D$_{i–iii}$).
418 Dark-rearing reduced relative TIMP2 expression in the GCL for *efemp1*$^{+/+}$ ($P = 0.0015$) but not
419 *efemp1*$^{2C\text{-}Cas9}$ fish, showing a gene-environment interaction ($P = 0.0069$; Fig 7D$_{i}$ and 7D$_{iv}$). At the 4-
420 week timepoint, overall dark-rearing reduced relative TIMP2 expression in the ACL and GCL (effect
421 of rearing conditions: $P = 0.0067$ and 0.0021, respectively; Fig 7E$_{1–4}$, 7E$_{i–ii}$ and 7E$_{iv}$). In the IPL, after
422 dark-rearing, relative TIMP2 expression seemed to be reduced in *efemp1*$^{2C\text{-}Cas9}$ fish but slightly
423 increased in *efemp1*$^{+/+}$ fish, exhibiting a gene-environment interaction ($P = 0.025$; Fig 7E$_{iii}$).

For MMP2, in the ACL, 2 days of dark-rearing overall resulted in higher MMP2 expression (effect of environment: $P = 0.0008$) in *efemp1*$^{+/+}$ fish but not in *efemp1*$^{2C\text{-}Cas9}$ fish (gene-environment interactions: $P = 0.0079$; Fig 7F$_{1–4}$ and 7F$_{i–ii}$). In the GCL, after 2 days of normal rearing, *efemp1*$^{+/+}$ fish had higher relative MMP2 expression than *efemp1*$^{2C\text{-}Cas9}$ fish ($P = 0.0064$; Fig 7F$_{1–2}$ and 7F$_{i–iv}$). 2 days of dark-rearing overall led to increased MMP2 expression in the GCL (effect of rearing conditions: $P < 0.0001$); this increase was greater in *efemp1*$^{2C\text{-}Cas9}$ than in *efemp1*$^{+/+}$ fish (effect of gene-environment interactions: $P < 0.0075$; Fig 7F$_{1–4}$, 7F$_{i}$ and 7F$_{iv}$). At the 4-week timepoint, MMP2 expression pattern was affected by dark-rearing, with lower relative expression in the ACL but higher expression in the IPL and GCL (effect of environment: $P < 0.0001$, $P = 0.0002$ and $P < 0.0001$, respectively; Fig 7G).

Overall, inner retinal distributions of EFEMP1, TIMP2 and MMP2 can be affected by either *efemp1* disruption or dark-rearing. More importantly, retinal *efemp1* modification impacts, in a time dependent manner, how dark-rearing-affects the redistribution of inner retinal proteins.

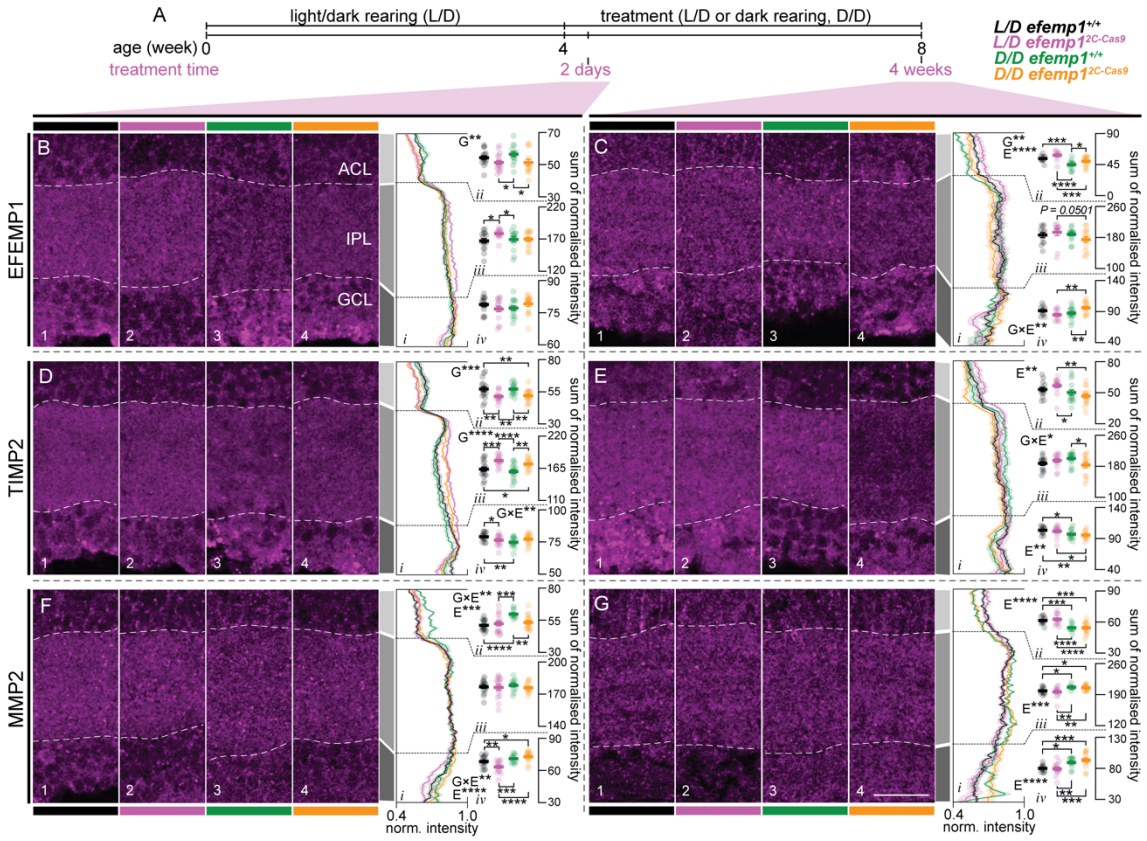

Figure 7. **Distribution of EFEMP1, TIMP2 and MMP2 in the inner retina of *efemp1*$^{+/+}$ and *efemp1*$^{2C\text{-}Cas9}$ fish after 2 days or 4 weeks of normal light/dark (L/D) cycle or dark (D/D) rearing. (A)** *Efemp1*$^{+/+}$ and *efemp1*$^{2C\text{-}Cas9}$ fish were reared under standard L/D condition to 4 weeks post-fertilization (wpf) and then were under L/D- or D/D-rearing to up to 8 wpf (4 weeks of treatment). Eyes for histological analysis were sampled after 2 days or 4 weeks of treatment. **(B–C)** Immunostaining for EFEMP1 to analyze its distribution in the inner retina, including amacrine cell layer (ACL), inner plexiform layer (IPL) and ganglion cell layer (GCL),

for L/D-reared *efemp1*$^{+/+}$, L/D-reared *efemp1*$^{2C\text{-}Cas9}$, D/D-reared *efemp1*$^{+/+}$ and D/D-reared *efemp1*$^{2C\text{-}Cas9}$ fish after 2 days (**B**; n = 16, 16, 14 and 14 retinae, respectively) and 4 weeks (**C**; n = 12, 12, 15 and 14 retinae, respectively) of treatment. White dash lines in micrographs highlight the borders of the IPL. Average normalized expression across the inner retina is shown in **(B_i and C_i)** and summed normalized expression (normalized intensity) for **(B_{ii} and C_{ii})** ACL, **(B_{iii} and C_{iii})** IPL and **(B_{iv} and C_{iv})** GCL was quantified for each eye. **(D–E)** Immunostaining for TIMP2 in the inner retina for L/D-reared *efemp1*$^{+/+}$, L/D-reared *efemp1*$^{2C\text{-}Cas9}$, D/D-reared *efemp1*$^{+/+}$ and D/D-reared *efemp1*$^{2C\text{-}Cas9}$ fish after 2 days (**D**; n = 16, 16, 16 and 15 retinae, respectively) and 4 weeks (**E**; n = 13, 14, 15 and 14 retinae, respectively) of treatment. Average normalized expression is shown in **(D_i and E_i)** and summed normalized expression for **(D_{ii} and E_{ii})** ACL, **(D_{iii} and E_{iii})** IPL and **(D_{iv} and E_{iv})** GCL. **(F–G)** Immunostaining for MMP2 for L/D-reared *efemp1*$^{+/+}$, L/D-reared *efemp1*$^{2C\text{-}Cas9}$, D/D-reared *efemp1*$^{+/+}$ and D/D-reared *efemp1*$^{2C\text{-}Cas9}$ fish after 2 days (**F**; n = 16, 16, 12 and 15 retinae, respectively) and 4 weeks (**G**; n = 13, 13, 12 and 15 retinae, respectively) of treatment. Average normalized expression is shown in **(F_i and G_i)** and summed normalized expression for **(F_{ii} and G_{ii})** ACL, **(F_{iii} and G_{iii})** IPL and **(F_{iv} and G_{iv})** GCL . Scale bar in **(G)** represents 20 µm and all images share the same scale. Group data are shown as mean ± SEM. *Two*-way ANOVA and Fisher's LSD *post-hoc* tests were performed. Significant main effects of genotypes (*G*), rearing conditions (*E*) and their interactions (*G*×*E*) are indicated in the graphs. **P < 0.05*; ***P < 0.01*; ****P < 0.001*; *****P < 0.0001*.

Discussion

In this study, we showed that retina-specific *efemp1* down-regulation leads to enlarged eyes and myopia development in zebrafish (Fig 2B, 2D–I). This resembles the progressive myopia that has been reported in human patients with loss-of-function *efemp1* mutations (Driver et al., 2020). However, mice with *efemp1* knockout showed no alternations in gross ocular structure, retinal function nor visual acuity, but did show progressive corneal maldevelopment (Daniel et al., 2020). Unfortunately, the authors did not analyze ocular refraction in their loss-of-function mouse model. In addition to aberrant eye growth, our mutants had reduced spatial visual sensitivity (Fig 1E–H, Fig S1) and altered retinal function (Figs 3 and 5). Particularly striking was the progressive slowing of the ERG in *efemp1*$^{2C\text{-}Cas9}$ fish with older ages (Fig 3 and 5). This resembles the age-related slowing of *b*-wave implicit time reported in some, but not all, human patients with Malattia Leventinese, a retinal dystrophy caused by a gain-of-function *efemp1* mutation (c.1033C>T, p.Arg345Trp) (Gerber et al., 2003). Taken together, *efemp1* mutant zebrafish show phenotype characteristics indicative of both gain- and loss-of-function mutations.

Concurrence of gain- and loss-of-function *efemp1* mutations in our mutants could be expected; with the 2C-Cas9 system, CRISPR gene editing independently occurred in retinal neurons expressing the Cas9 nuclease, leading to different types of indels even within an individual retina. Despite these mutations being mosaic and perhaps of low efficiency (Fig 1C–D) in our model, the phenotype was robust, indicating that tight control of finely balanced *efemp1* expression is required for optimal ocular development. However, this does demonstrate the importance of using the 2C-Cas9 system with caution for studies requiring specific gain- or loss-of-function mutations. To avoid such heterogeneous tissue-

477 specific gene editing, the Cre-LoxP system is an option: using tissue-specific driven Cre recombination
478 to delete LoxP flanked exons of the target gene. Our data showed a down-regulation of *efemp1* in
479 *efemp1*$^{2C\text{-}Cas9}$ fish at 8 weeks of age (Fig 6B). In contrast, a recent study reported increased EFEMP1 in
480 tears sampled from myopic human patients and increased EFEMP1 in myopic guinea pig choroid (Shi
481 et al., 2023). To understand these species related differences, tissue specific comparative studies would
482 be required.

483 We noticed that although 5 dpf *efemp1*$^{2C\text{-}Cas9}$ fish overall were not myopic relative to *efemp1*$^{+/+}$ fish (Fig
484 2B), they showed reduced spatial-frequency tuning function (Fig 1E–H). This phenotype, if not due to
485 refractive error, can be a result of altered visual processing, as aberrant extracellular matrix caused by
486 *efemp1* disruption may lead to dysfunctional synapses (Dityatev and Schachner, 2006).

487 For our ERG results, although slower ERG responses were a robust phenotype in *efemp1*$^{2C\text{-}Cas9}$ fish at
488 the older ages, at 2 wpf *a*- and *b*-wave implicit times were actually faster than control *efemp1*$^{+/+}$ fish
489 (Fig 3A$_3$–A$_4$). One possible explanation is that *efemp1*$^{2C\text{-}Cas9}$ fish had shorter axial length than *efemp1*$^{+/+}$
490 fish at this age ($P < 0.0001$, unpaired *t*-test; Fig S2) and thus effectively higher retinal illumination.

491 We noticed that under normal rearing, *efemp1*$^{2C\text{-}Cas9}$ fish had larger *a*-wave amplitudes at 8 wpf (or 4-
492 week timepoint in the dark-rearing experiment) than *efemp1*$^{+/+}$ fish, which we attributed to slower *b*-
493 wave onset exposing more of the *a*-wave (Fig 3D$_2$ and Fig 5V). *B-wave* effects in 8 wpf *efemp1*$^{2C\text{-}Cas9}$
494 fish were less consistent, with slightly higher *b*-wave amplitudes in one experiment (Fig 3D$_1$) but
495 smaller *b*-waves in another (Fig 5U). We speculated that this might arise from variability in gene editing
496 (as discussed above) between retinae (and batches), leading to different severities and phenotypes.
497 Nonetheless, it is clear that *efemp1* function causes retinal dysfunction in zebrafish.

498 Under dark-rearing, retinal dysfunction in *efemp1*$^{2C\text{-}Cas9}$ was exacerbated (Fig 5), but this did not lead to
499 worsening myopia (Fig 4). One speculation is that without visual input (dark-rearing) in the presence
500 of *efemp1* disruption the zebrafish eye shuts down light-dependent signals for ocular growth and
501 switches to intrinsic mechanisms for ocular growth regulation, thus leading to emmetropic vision. This
502 idea requires investigation.

503 Our survival analysis suggested that *efemp1*$^{2C\text{-}Cas9}$ mutants at 4 wpf did not show a myopic shift. This
504 could be due to a number of factors. Firstly, because those fish with a higher level of visual impairment
505 and perhaps early-onset myopia are those likely to have been lost by 4 wpf. Thus, those fish with lower
506 mutation rates and better vision were more likely survived to older ages allowing more time (>4 weeks)
507 for the development of myopia (Fig 2C). Secondly, changes in *egr1* expression shown in our data (Fig
508 6C) may also be a separate contributor to the observed absent myopic shift in 4 wpf *efemp1*$^{2C\text{-}Cas9}$ fish.
509 Previous studies suggest that *egr1* may have a role in signaling bi-directional ocular growth (Ashby et
510 al., 2014; Fischer et al., 1999). Up-regulated *egr1* expression in 2-day normal-light-reared (~4 wpf)
511 *efemp1*$^{2C\text{-}Cas9}$ fish showed evidence myopia suppression, whereas down-regulation of *egr1* in 4-week
512 normal-light-reared (equivalent to 8 wpf) *efemp1*$^{2C\text{-}Cas9}$ fish showed a myopic shift (Fig 6C). The
513 direction of these expression changes qualitatively matched ocular refraction of *efemp1*$^{2C\text{-}Cas9}$ fish at the
514 corresponding ages (Fig 2B).

515 In our gene expression data, down-regulation of *tgfb1a* and *vegfab* was associated with myopia
516 development in *efemp1*$^{2C\text{-}Cas9}$ fish under normal lighting (Fig 6E and 6G) (Jobling et al., 2004; Zhu et
517 al., 2021). Dark-rearing-induced down-regulation of *egr1*, *tgfb1s*, *vegfaa*, *fgf2* and *rbp3*, and up-
518 regulation of *gjd2b* were not impacted by *efemp1* modification (Fig 6C, 6D–F, 6I, 6K and 6M), with
519 two exceptions being *vegfab* and *wnt2b* (Fig 6G and 6J). Despite the similarities in dark-rearing-induced
520 gene expression, *efemp1*$^{+/+}$ fish became myopic after 4 weeks of dark-rearing, *efemp1*$^{2C\text{-}Cas9}$ fish
521 remained emmetropic (Fig 4). It is possible that *efemp1* functional integrity is required to manifest
522 dark-rearing-induced phenotypes with changes in these genes. We speculate that without normal *efemp1*
523 expression under dark-rearing, intrinsic mechanisms may take over and regulate ocular growth. Future
524 investigations are required to verify this hypothesis.

525 The genes *wnt2b* (Fig 6J) and *vegfab* (Fig 6 G), were down-regulated only in *efemp1*$^{+/+}$ but not *efemp1*$^{2C\text{-}}$
526 ^{Cas9} fish after 2 days and 4 weeks of dark-rearing, respectively, suggesting that dark-rearing requires
527 normal *efemp1* expression to induce and maintain their expression changes, respectively. EFEMP1 has
528 been previously shown to suppress the epithelial-mesenchymal transition in endometrial carcinoma
529 through Wnt/β-catenin signaling, for which WNT2B is an activator (Blomfield et al., 2023; Yang et al.,

530 2016). Further investigation might target interactions between EFEMP1, WNT2B and EMT in myopia
531 development. Importantly, the impact of *efemp1* modification on dark-rearing-induced *vegfab*
532 expression further implies a light-dependent signaling between *efemp1* and *vegfab* that is crucial for
533 ocular growth.

534 There was up-regulation of *rbp3* expression in normal-light-reared *efemp1*$^{2C\text{-}Cas9}$ fish at the 2-day but
535 not at the 4-week timepoint (Fig 6K). It is likely that *efemp1* deficiency altered the interphotoreceptor
536 matrix and thus impairing the visual cycle and *11-cis* retinal supply (Gonzalez-Fernandez and Ghosh,
537 2008; Yue, 2014). Up-regulating *rbp3* may be a compensatory response in young zebrafish. Myopia
538 development has been reported in *gjd2b* knockout zebrafish (Quint et al., 2021), however our data
539 showed robust *gjd2* up-regulation in both phenotypes under myopia-inducing dark-rearing (Fig 6M).
540 Whether this up-regulation reflect feedback remains to be clarified.

541 In our histological analysis, distribution changes of EFEMP1 in the inner retina under different rearing
542 conditions indicate retinal *efemp1* modification at the post-transcriptional level (Fig 7B–C). In addition,
543 our data indicated that *efemp1* modification affects the way that inner retinal MMP2 (particularly after
544 2 days) and TIMP2 (particularly after 4 weeks) were impacted in response to dark-rearing (Fig 7D–G).
545 There have been previous reported that changes in expression of EFEMP1 in cultured endothelial cells
546 led to decreased MMP2 but unchanged TIMP2 expression (Albig et al., 2006), highlighting a context-
547 dependent regulation of EFEMP1. In future studies, it will be worth analyzing other MMPs (e.g., MMP3,
548 etc.) and TIMPs (e.g., TIMP1 and TIMP3, etc.) that have been associated with EFEMP1 (Livingstone
549 et al., 2020) and eye elongation (Jia et al., 2017; Jia et al., 2014).

550 In summary, the modification of retinal *efemp1* in zebrafish resulted in reduced spatial visual sensitivity,
551 axial myopia, eye enlargement, altered retinal function, myopia-associated gene expression changes
552 (i.e., *egr1*, *efemp1*, *tgfb1a*, *vegfab*, *rbp3*), and redistribution of inner retinal EFEMP1, TIMP2 and
553 MMP2 proteins, under normal rearing. Under dark-rearing, *efemp1*$^{2C\text{-}Cas9}$ fish did not develop myopia,
554 even though dark-rearing seemed to worsen retinal function. We found *efemp1*-dependent responses of
555 *vegfab* and *wnt2b* expression to dark-rearing, highlighting signaling between *efemp1* and these genes
556 as likely mechanisms involved in visually regulated ocular development. Dark-rearing-induced

557 redistribution of EFEMP1, TIMP2 and MMP2 were also influenced by *efemp1* disruption. This study
558 provides robust evidence that *efemp1* regulates ocular development and visual function in a light-
559 dependent manner, with several potential myopia-associated molecular pathways implicated for further
560 investigation. We illustrated a valuable zebrafish analysis platform combining environmental and
561 genetic manipulations, as well as multifaced analyses for high-throughput investigation of the growing
562 number of myopia-risk genes to gain insight into their interactions with visual environment in myopia
563 development.

564

565 Materials and Methods

566 Animal husbandry

567 All procedures were performed according to the provisions of the Australian National Health and
568 Medical Research Council code of practice for the care and use of animals and were approved by the
569 Faculty of Science Animal Ethics Committee at the University of Melbourne (Project No. 10399).

570 For standard husbandry, zebrafish (Danio rerio; transgenic fish, see detailed description below) were
571 maintained and bred in the Fish Facility at the University of Melbourne according to local animal
572 guidelines. Embryos and larvae (prior to sex determination) were grown in Petri dishes in an incubator
573 at 28.5°C up to 5 days post-fertilization (dpf), then introduced to tanks under normal 14h/10h light/dark
574 (L/D) cycles and raised in flow-through systems at 28°C.

575 For dark (D/D) rearing, zebrafish tanks were wrapped using black cloth tapes (Model number
576 66623336603; Bear brand, Saint-Gobain Abrasives, Somerton, VIC, Australia) to block light. Zebrafish
577 were induced to blackout tanks at 4 wpf and reared in darkness for 2 days, 2 or 4 weeks. Age-matched
578 fish reared under standard lighting were used as environmental control. Zebrafish health condition and
579 survival were monitored daily using dim red light (LED; 17.4 $cd.m^{-2}$, λ_{max} 600 nm).

580

581 Generation of mutants

582 In this study, we used a novel somatic CRISPR gene editing system, namely 2C-Cas9 (Di Donato et al.,
583 2016), to generate retina-specific *efemp1* mutation in zebrafish. The
584 p*UAS*:*Cas9T2ACre*;*U6*:*sgRNA1*;*U6*:*sgRNA2* plasmid (Addgene #74010) was digested using BsaI
585 (R0535S; NEB, Ipswich, MA, USA) and BsmBI-v2 enzymes (R0739S; NEB) targeting the restriction
586 sites behind the U6 promoters to remove the pre-set sequences that are to be replaced by DNA sequences
587 of small guide RNA (sgRNA). Digested vectors were purified using a QIAquick Gel Extraction kit
588 (28704; Qiagene, Hilden, Germany). Double-strand DNAs of the two sgRNAs (oligos shown in Table
589 S2), *efemp1sgRNA1* and *efemp1sgRNA2*, were annealed from single-strand oligos and inserted into the
590 digested vector using T4 DNA ligase (M0467S; NEB). Ligated plasmids were transformed into α-select
591 chemically competent cells (BIO-85026; Bioline, London, UK). Positively transformed cells were
592 selected using antibiotic Ampicillin LB agar plates and colonies were picked to grow in Ampicillin LB
593 medium at 37°C for overnight. Plasmids were extracted and purified using a QIAprep Spin Miniprep
594 kit (27106; Qiagene). Successful insertions of DNAs into the plasmid were determined by sequence-
595 specific PCR, gel electrophoresis and Sanger sequence (Fig S3B). Concentrations of extracted plasmids
596 were quantified using a Nanodrop 1000 (Thermo Fisher Scientific; Waltham, MA, USA). *Efemp1*
597 sgRNAs targeting exons were designed based on the *efemp1* genome DNA sequence (gDNA;
598 ENSDARG00000059121) using the *CHOPCHOP* online tool (Labun et al., 2019) and pre-tested *in*
599 *vitro* using a GenCrispr sgRNA Screening kit (Fig S3A;L00689; GenScript, NJ, USA) before insertion
600 into vectors. The two sgRNAs target exons 3 and 5 of *efemp1* gDNA. Tol2 transposase mRNA was
601 transcribed from a p*tol2* plasmid (kind gift from Dr. Mirana Ramialison, Murdoch Children's Research
602 Institute) using a mMESSAGE mMACHINE SP6 Transcription Kit (AM1340; Thermo Fisher
603 Scientific).

604 To generate the retina-specific *efemp1* modification in zebrafish, we co-injected
605 p*UAS*:*Cas9T2ACre*;*U6*:*efemp1sgRNA1*;*U6*:*efemp1sgRNA2* at a concentration of 35 ng/µl and *tol2*
606 mRNA at 50 ng/µl into embryos of fish Tg(*bact2-loxP-mCherry-loxP-eGFP*) × Tg(*rx2*:*Gal4*).
607 Expression of the injected plasmid were identified based on green fluorescence (eGFP) in the zebrafish
608 eyes observed under a fluorescence microscope at 3 dpf. F0 fish with green fluorescent eyes were mated

609 with transgenic fish Tg(*bact2-loxP-mCherry-loxP-eGFP*) × Tg(*rx2*:*Gal4*) to screen for the founders
610 that had the 2C-Cas9 transgene integrated into the germ line. In this study, we used transgenic fish
611 Tg(*bact2-loxP-mCherry-loxP-eGFP*) × Tg(*rx2*:*Gal4*), namely *efemp1*$^{+/+}$ fish as the control of the
612 mutant fish Tg(*bact2-loxP-mCherry-loxP-eGFP*) × Tg(*rx2*:*Gal4*) ×
613 Tg(*UAS*:*Cas9T2ACre*;*U6:efemp1sgRNA1*;*U6:efemp1sgRNA2*), named *efemp1*$^{2C\text{-}Cas9}$ fish. These fish
614 also have a transgene Tg(*UAS*:*nfsb-mCherry*) that was driven by the retina-specific Tg(*rx2*:*Gal4*),
615 leading to much brighter red fluorescence signals in the zebrafish eye than in the body, where *mCherry*
616 expression was triggered by Tg(*bact2-loxP-mCherry-loxP-eGFP*). These allowed to sort Tg(*rx2*:*Gal4*)
617 positive fish for *efemp1*$^{+/+}$ fish. *Efemp1*$^{2C\text{-}Cas9}$ fish were sorted by eye-specific green fluorescence, which
618 indicated presence of Tg(*rx2*:*Gal4*), without the need to the Tg(*UAS*:*nfsb-mCherry*) reporter. However,
619 to ensure that the only genetic difference between *efemp1*$^{+/+}$ and *efemp1*$^{2C\text{-}Cas9}$ fish was from the 2C-
620 Cas9 construct Tg(*UAS*:*Cas9T2ACre*;*U6:efemp1sgRNA1*;*U6:efemp1sgRNA2*), we also used fish with
621 bright red eyes indicating existence of Tg(*UAS*:*nfsb-mCherry*) for mutant groups. As the Tg(*UAS*:*nfsb-*
622 *mCherry*) was not directly relevant to the 2C-Cas9 gene editing system and our phenotypic assessments,
623 for a simplified demonstration, we did not highlight this transgene construct in this report.

624 For genotyping, we used a headloop PCR protocol (Kroll et al., 2021). Standard PCR Primers were
625 designed using Primer Premier 5.0 (Singh et al., 1998) and headloop PCR primers were designed using
626 a published Python script (Kroll et al., 2021) (see Table S3 for oligo information). GDNA was isolated
627 from 7 dpf *efemp1*$^{+/+}$ or *efemp1*$^{2C\text{-}Cas9}$ zebrafish eyes using a Monarch Genomic DNA Purification Kit
628 (T3010S; NEB) and quantified using a Nanodrop 1000 (Thermo Fisher Scientific). In a PCR reaction,
629 there were 30 ng gDNA of either genotype, 0.25 µl 10 mM forward primer, 0.25 µl 10 mM reverse
630 primer, 5 µl Hot Start High-Fidelity 2× Master Mix (M0494S; NEB) and nuclease-free water to fill up
631 to 10 µl. The PCR program was comprised of an initial denaturation step of 98°C for 30 seconds, 32
632 cycles of 98°C for 15 seconds, 60°C for 15 seconds, and 72°C for 15 seconds, followed by a final
633 extension step of 72°C for 2 minutes. Electrophoresis of the PCR products was performed using 2%
634 Tris-acetate-EDTA (TAE) agarose gel.

635

636 **Optomotor response (OMR)**

637 The OMR apparatus was adapted from that previously described (Xie et al., 2019a; Xie et al., 2021;
638 Xie et al., 2019b). A Power Mac G5 computer (Apple Computer, Inc., Cupertino, CA, USA) ran
639 MATLAB 2016b (MathWorks, Natick, MA, USA) with Psychtoolbox extensions (Kleiner et al., 2007).
640 Stimuli were processed on an ATI Radeon HD 5770 graphics card, with the output sent to a BITS++
641 video processor (Cambridge Research Systems, Rochester, UK) for increased contrast resolution for
642 stimuli displayed on a M992 flat-screen cathode ray tube (CRT) monitor (Dell Computer Corporation,
643 Round Rock, TX, USA) with its screen facing upwards. During experiments, a zebrafish was placed in
644 a custom annulus swimming chamber (the inner and outer walls were 29.5 and 46.5 mm from the center,
645 respectively) with a transparent base positioned 46 mm above the screen. A C922 Pro Stream webcam
646 (Logitech Company, Lausanne, Switzerland; 1080p at 30 Hz), placed 130 mm above the swimming
647 chamber base, controlled using MATLAB recorded videos of each trial for *post-hoc* analysis of
648 zebrafish angular movement.

649 During a trial, a test stimulus was displayed on the CRT screen below the swimming chamber, rotating
650 at 0.5 rad/s for 30s. Test stimuli were windmill sinusoidal gratings with central spatial frequencies of
651 0.0078, 0.0155, 0.0310, 0.0620, 0.1240 and 0.2480 cycle per degree (c/°). A blank grey screen was
652 presented between test stimuli. Test stimuli were generated using the green and blue channels of the
653 CRT monitor with constant red luminance across the screen. A long pass filter (cut-off wavelength
654 600nm) was fixed to the front of a camera to filter out blue and green light, allowing only red light to
655 pass through, thus eliminating the moving stimulus and allowing better visualization of the fish for
656 analysis.

657 OMR was measured for 5 dpf and 2 wpf *efemp1*$^{+/+}$ and *efemp1*$^{2C\text{-}Cas9}$ zebrafish, after acclimating fish to
658 the swimming chamber for 5 minutes. All experiments were conducted between 9:00 AM and 7:00 PM.
659 After experiments, fish were humanely killed using 1000 ppm AQUIS (#106036, Primo Aquaculture).

660 The position of zebrafish during each trail was tracked using a published python package *Stytra* (Štih
661 et al., 2019). Using custom MATLAB algorithms, we calculated the overall angular movement of
662 zebrafish in the direction of the rotating grating for each trial as the optomotor index (OMI). For each

663 fish, OMI at a spatial frequency was averaged from results of 4 trials (2 repeats at either clockwise or
664 counter-clockwise direction). 5 dpf OMI data were normalized to the averaged OMI of *efemp1*$^{+/+}$ fish
665 at 0.0155 c/° (i.e., the condition for which 5 dpf zebrafish showed the greatest response) and 2 wpf OMI
666 data were normalized to averaged OMI of *efemp1*$^{+/+}$ fish at 0.0620 c/° (i.e., the condition for which 2
667 wpf zebrafish showed the greatest response). The spatial-frequency tuning functions were fit using a
668 log-Gaussian using a least-squares criterion to return amplitude (i.e., height of the peak), peak spatial
669 frequency (i.e., spatial frequency at which amplitude peaked), and bandwidth (i.e., standard deviation).
670 To test whether spatial-frequency tuning functions differed between groups, an omnibus *F*-test was
671 used to compare the goodness of fit (r^2) of a full model, in which parameter estimates of each group
672 could vary independently, with that of a restricted model, in which parameters were constrained to be
673 the same across groups. To determine whether specific parameter estimates differed between groups, a
674 nested *F*-test was used to compare a full model with a restricted model in which one parameter was
675 constrained to be the same across groups (Lu and Dosher, 2013). A criterion of $\alpha = 0.05$ was used to
676 determine significance.
677

678 **Optical coherence tomography (OCT)**

679 OCT was performed immediately after zebrafish were humanely killed using 1000 ppm AQUI-S
680 (#106036, Primo Aquaculture) in E3 medium. Zebrafish were positioned on a square (2 × 2 cm) of
681 paper towel and transferred onto a moistened PVA sponge fitted snugly in a 35-mm Petri dish. All OCT
682 images were recorded using a spectral domain OCT/OCTA system (Spectralis OCT2; Heidelberg
683 Engineering, Heidelberg, Germany) with the aid of a Digital High Mag lens (78D, Volk Optical Inc.,
684 Mentor, Ohio, USA) attached. The Petri dish was then affixed vertically onto a platform, allowing the
685 zebrafish eye to be aligned with the lens. Surface tension between the moistened sponge/paper towel
686 and the fish kept it in place. Images were acquired in the dorsal-ventral direction with a volume scan
687 pattern of 15° × 5° (2.7 × 0.9 mm). Each volume consisted of 128 B-scans (5 repeats) each consisting
688 of 512 A-scans. When imaging, the OCT was positioned such that the iris was horizontal, and a bright
689 reflection can be seen at the apex of the cornea. This ensured that the image captured was aligned with

690 the central axis of the eye. As myopia can independently develop in an eye without signals from the
691 brain (Troilo et al., 1987), and thus the other eye, both eyes were imaged for each zebrafish in our study.

692 Only for 5-dpf fish, eyes were imaged using a Bioptigen Envisu R2200 spectral domain OCT system
693 with an 18-mm telecentric lens (Bioptigen Inc., Durham, NC), due to temporary unavailability of the
694 Spectralis OCT system. The position of the sponge platform with a zebrafish (as described above) was
695 carefully adjusted to ensure that the central apex was aligned with the objective lens. A volume scan of
696 2 × 2 mm was acquired with a depth of 1.7 mm (1000 A-scans per B-scans).

697 Image quantification was performed using a custom MATLAB script. Axial length is quantified as the
698 distance from the corneal apex to the retinal pigment epithelium (RPE). Lens radius is half of the
699 distance from the anterior to posterior lens surface. The retinal radius is the distance from the center of
700 the lens to the RPE, which indeed can be calculated as the difference between axial length and lens
701 radius (Fig 2A). With these parameters, relative axial ocular refraction is given by the ratio of retinal
702 radius to lens radius (*Matthiessen's Ratio*), which is commonly used for analyzing ocular refraction of
703 aquatic species (Collery et al., 2014; Shand et al., 1999; Turnbull et al., 2015). *Two*- or *three*-way
704 ANOVA with Fisher's LSD tests were performed in Prism 9 (GraphPad, San Diego, CA, USA) and a
705 criterion of $\alpha = 0.05$ was used to determine statistical significance.

706

707 **Survival comparison between *efemp1*$^{2C\text{-}Cas9}$ fish with different eGFP levels**

708 *Efemp1*$^{2C\text{-}Cas9}$ fish were sorted under a fluorescence microscope and divided to two groups based on the
709 intensity of the retinal eGFP fluorescence; fish with weak eGFP signals were classified to eGFP+ group
710 and those with strong eGFP fluorescence were categorized to the eGFP+++ group. *Post-hoc* retinal
711 histology indicated that intensity of eGFP fluorescence is corresponding to eGFP positive cell number;
712 fish with higher eGFP fluorescence level had more eGFP positive cells. Both groups were reared under
713 standard husbandry and their survival was recorded at 2, 4, 6 and 8 weeks of age. There were 3 tanks
714 for both groups (37–60 fish each tank at 5 dpf). *Two*-way ANOVA and Fisher's LSD *post-hoc* analyses
715 were performed in Prism 9. A criterion of $\alpha = 0.05$ was used to determine significance.

716

717 **Electroretinography (ERG)**

718 The procedure for scotopic ERG was adapted from our published method (Xie et al., 2019c). Fish were
719 dark adapted (>8 hours, overnight) prior to experiments. All procedures were conducted under dim red
720 illumination (17.4 cd·m^{-2}; λmax = 600 nm). For recording, a fish was humanely killed by immersing in
721 0.1% tricaine MS-222 (E10521; Sigma-Aldrich, St. Louis, MO, USA) in E3 medium. When gills had
722 stopped moving and fish were unresponsive response to a gentle touch, the head was removed and
723 immediately rinsed in E3 medium. The eyes were quickly dissected using fine-tipped tweezers under a
724 dissecting microscope. A small incision was made around the central cornea for each eye to allow a
725 small amount of aqueous humor to flow out. This helps keep the recording electrode to stay moist,
726 increasing conductivity and minimizing noise. The dissected eyes were moistened with multiple drops
727 of E3 medium using a 3-mm Pasteur pipette. The eyes were then transferred onto a square of paper
728 towel (2 × 2 cm) on a moist polyvinyl alcohol (PVA) sponge platform in a Faraday cage. Both eyes
729 were measured at the same time. For recording from eyes at or older than 4 wpf, recording electrodes
730 were 0.3-mm chloride-electroplated silvers (99%). For younger eyes, a moistened cone-shape sponge
731 (tip diameter ~40 μm) was attached to the silver. Under a microscope, the recoding electrodes were
732 positioned to gently touch the central corneal apex, and the reference electrodes were inserted into the
733 sponge platform. After electrode placement, the Ganzfeld bowl was moved to cover the platform, and
734 the eyes were allowed to dark adapt for 3 minutes. ERG responses for each fish were recorded with
735 flash stimuli of –2.11, –0.81, 0.72, 1.89 and 2.48 to analyze the impact of *efemp1* modification on retinal
736 function during normal development, and at −0.83, 0.73 and 1.87 log cd·s·m^{-2} for examining how
737 *efemp1* modification impact fish's retinal physiological changes in response to myopia-inducing dark-
738 rearing. For stimulus intensities at or lower than 0.73 log cd·s·m^{-2}, three repeats were measured with
739 an inter-flash interval of 15 seconds and there was a 30-second interval between intensities. For stimulus
740 intensities at or higher than 1.87 log cd·s·m^{-2}, a single response was measured with a 60-second re-
741 adaption to dark before the flash.

742 All experiments were performed between 9:00 AM and 7:00 PM at room temperature. Amplitudes of
743 the *a*- and *b*- waves were measured from baseline to the negative *a*-wave trough and from the negative

744 *a*-wave trough to the *b*-wave peak, respectively. Implicit times of the *a*- and *b*-waves were measured
745 from stimulus onset to the *a*-wave trough and the *b*-wave peak, respectively. *Two*- or *three*-way
746 ANOVA, and Fisher's LSD *post-hoc* tests were performed in Prism 9. A criterion of $\alpha = 0.05$ was used
747 to determine significance.

748

749 **Gene expression analysis**

750 Zebrafish were humanely killed by 1000 ppm AQUIS (#106036, Primo Aquaculture) and stored in
751 RNALater (AM7020, Thermo Fisher, Waltham, MA, USA) at –20°C if not immediately used for RNA
752 isolation. For RNA isolation, eyes were dissected from zebrafish and lenses were removed. For each
753 sample, the total RNA of 4 eyes from two fish was isolated using TRIzol (or TRI-reagent; AM9738,
754 Thermo Fisher scientific) (Rio et al., 2010) and quantified using a Nanodrop 1000 (Thermo Fisher
755 Scientific). 750 ng (2 days of treatment) or 1 µg (4 weeks of treatment) of the total RNA was reverse-
756 transcribed into cDNA using a Tetro cDNA synthesis kit (BIO-65042, Bioline). Quantitative PCR (RT-
757 qPCR) assays were performed on a CFX96 real-time PCR system (Bio-Rad, Hercules, CA, USA) using
758 SsoAdvanced Universal SYBR Green Supermix (12 µL final mix per reaction; 1725272, Bio-Rad). In
759 this study, mRNA levels of *egr1*, *efemp1*, *tgfb1a*, *tgfb1b*, *vegfaa*, *vegfab*, *igf1*, *fgf2*, *wnt1b*, *rbp3*, *gjd2a*
760 and *gjd2b* were quantified. Primers of the tested genes were as listed in our previous study (Xie et al.,
761 2023 Preprint). A housekeeping gene *elongation factor 1-alpha* (*ef1a*) served as an internal control
762 (McCurley and Callard, 2008). For each gene, there were 4 samples per group and 3 replicates per
763 sample. Calculation of expression levels was performed using the $2^{-\Delta\Delta CT}$ method (Livak and Schmittgen,
764 2001) and the transcript levels were normalized to the *ef1a* transcript levels in L/D-reared *efemp1*$^{+/+}$
765 eyes at each time point. For statistics, *two*-way ANOVA and Fisher's LSD *post-hoc* tests were
766 performed in Prism 9. A criterion of $\alpha = 0.05$ was used to determine significance.

767

768 **Histology**

769 For Immunohistochemistry, whole zebrafish (if at 2 weeks of age) or dissected zebrafish eyes (if older
770 than 2 weeks of age; lenses excluded) were fixed in 4% paraformaldehyde (PFA) in PBS for 48 hours

771 at 4°C. They were cryoprotected in 30% sucrose in PBS, embedded in Tissue-Tek OCT compound
772 (Sakura Finetek, Torrance, CA, US) and cryosectioned (20 µm of thickness; CM 1860 Cryostat; Leica,
773 Wetzlar, Germany). Antibody staining was carried out at room temperature using standard protocols.
774 Slides were blocked in 5% fetal bovine serum (FBS) for 30 minutes and incubated overnight in rabbit
775 anti-EFEMP1 (ARP41450_P050, 1:600; Sapphire Bioscience, NSW, Australia), sheep anti-TIMP2
776 (1:1000; kind gift from the Itoh Lab at the University of Oxford, UK) or rabbit anti-MMP2 (AS-55111,
777 1:250; AnaSpec, Fremont, CA, USA) primary antibodies diluted in FBS. Noting that the anti-EFEMP1
778 antibody does not bind to EFEMP1 regions corresponding to sgRNAs target sites on zebrafish *efemp1*
779 DNA, thus mutant proteins (if any) may still be labeled by the antibody. The anti-TIMP2 antibody was
780 developed based on human TIMP2. In a previous study this antibody was showed to label for zebrafish
781 TIMP2a (Zhang et al., 2003). As similarity of zebrafish TIMP2b to human TIMP2 is much lower than
782 that of zebrafish TIMP2a (60.55% vs. 71.23%), labelling of zebrafish TIM2b is less likely. Yet, we are
783 not able to completely rule out this possibility due to lack of information of the exact immunogen. Slides
784 were subsequently incubated for 2 hours in secondary antibodies (all 1:500; Thermo Fisher Scientific)
785 diluted in FBS. The secondary antibodies used were Chicken anti-Rabbit Alexa Fluor 647 (A21443) or
786 Donkey anti-Sheep Alexa Fluor 647 (A21448). Nuclei were counterstained with 4′ ,6-diamidino-2-
787 phenylindole (DAPI; D9542-10MG, 1:10000; Sigma-Aldrich) in PBS for 20 minutes, and sections were
788 mounted in Mowiol (81381-250G; Sigma-Aldrich). Stained sections were imaged at a distance 100 µm
789 from the center of the optic nerve, using a Nikon A1R confocal microscope (Nikon, Minato City, Tokyo,
790 Japan) with a 40× air objective lens (NA 0.95). For all confocal imaging, the deconvolution function of
791 the NIS elements software (AR4.6, Nikon) was applied to minimize background noise. Image
792 brightness and contrast were adjusted using Photoshop (Adobe, San Jose, CA, USA) or FIJI (Schindelin
793 et al., 2012).

794 To analyze the relative distribution of EFEMP1, TIMP2 and MMP2, images were pre-processed in FIJI.
795 In each image, an inner retinal region was selected by drawing a line that followed the contour of the
796 inner plexiform layer (IPL) with a line thickness of 1000 pixels, which includes the inner nuclear layer
797 (INL; including the amacrine cell layer, ACL), IPL and ganglion cell layer (GCL). This line allowed

798 the retinal cross section to be straightened using the 'Straighten' function. The duplicated images
799 returned were rotated, positioning the INL on the left and GCL on the right. The widths of the
800 straightened images were then resized using Adobe Photoshop to normalize the IPL thickness to the
801 averaged IPL thickness of the control group (L/D-reared *efemp1*$^{+/+}$ fish) relevant to that timepoint.
802 Regions of interest (ROI) boxes measuring 150-pixel height and widths of 390 (2-day L/D- or DD-
803 reared *efemp1*$^{+/+}$ and *efemp1*$^{2C\text{-}Cas9}$ fish) or 455 pixels (4-week L/D- or DD-reared *efemp1*$^{+/+}$ and
804 *efemp1*$^{2C\text{-}Cas9}$ fish) were used to return expression levels using the '*Plot Profile*' function in FIJI. For
805 each image, brightness profiles across the ACL, IPL and GCL were normalized to the highest value. To
806 examine relative change in the three layers, normalized intensity was summed throughout the ACL
807 (pixel 1–90), IPL (2-day: pixel 91–300; 4-week: pixel 91–330) and GCL (2-day: pixel 301–390; 4-week:
808 pixel 331–455) for each image. One section per retina was used and both eyes from a zebrafish were
809 taken for analysis in this study. *Two*-way ANOVA and Fisher's LSD *post-hoc* tests were performed in
810 Prism 9 and a criterion of $\alpha = 0.05$ was used to determine statistical significance.

811

812 **Data availability**

813 All data have been made available on Open Science Frame (https://osf.io/rdmvy/).

814

815 **Acknowledgments**

816 We thank Yoshi Itoh for his kind gift of a sheet anti-TIMP2 antibody and Dr. Mirana Ramialison for
817 providing the p*Tol2* plasmid. We thank the Biological Optical Microscopy Platform (BOMP) at the
818 University of Melbourne for providing instrument for confocal imaging. We acknowledge the staff of
819 the Danio rerio University of Melbourne, and Walter and Eliza Hall of Medical Institute fish facilities
820 for animal husbandry and support.

821 JX was supported by the Melbourne Research Scholarship for his PhD study the Dr Albert Shimmins
822 Postgraduate Writing-Up Award for manuscript preparation. Funding was provided through the
823 University of Melbourne research grant support scheme and an international collaborative fund from
824 Research Centre for SHARP vision (RCSV), The Hong Kong Polytechnic University.

Author Contributions

Conceptualization, JX, BVB, PTG, PJ; Methodology, JX, BVB, PTG, PJ; Data collection, JX; Writing – Original Draft, JX; Writing – Review & Editing, JX, BVB, PJ; Data analysis and visualization, JX; Supervision, BVB, PTG, PJ; Project Administration, PJ; Funding Acquisition, PJ.

Disclosure and competing interests statement

The authors declare no conflict of interest.

833 ## References

834 Albig, A.R., J.R. Neil, and W.P. Schiemann. 2006. Fibulins 3 and 5 Antagonize Tumor Angiogenesis In vivo.
835 *Cancer Res* 66:2621-2629 10.1158/0008-5472.Can-04-4096.
836 An, J., E. Hsi, X. Zhou, Y. Tao, S.-H.H. Juo, and C.-L. Liang. 2012. The FGF2 gene in a myopia animal model and
837 human subjects. *Molecular Vision* 18:471
838 Ashby, R.S., G. Zeng, A.J. Leotta, D.Y. Tse, and S.A. McFadden. 2014. Egr-1 mRNA Expression Is a Marker for the
839 Direction of Mammalian Ocular Growth. *Investigative Ophthalmology & Visual Science* 55:5911-5921
840 10.1167/iovs.13-11708.
841 Bikfalvi, A., S. Klein, G. Pintucci, and D.B. Rifkin. 1997. Biological Roles of Fibroblast Growth Factor-2*.
842 *Endocrine Reviews* 18:26-45 10.1210/edrv.18.1.0292.
843 Blomfield, A.K., M. Maurya, K. Bora, M.C. Pavlovich, F. Yemanyi, S. Huang, Z. Fu, A.E. O'Connell, and J. Chen.
844 2023. Ectopic Rod Photoreceptor Development in Mice with Genetic Deficiency of WNT2B. *Cells*
845 12:1033
846 Bloomfield, S.A., and B. Völgyi. 2009. The diverse functional roles and regulation of neuronal gap junctions in
847 the retina. *Nature Reviews Neuroscience* 10:495
848 Chuang, J.C., and P.A. Raymond. 2001. Zebrafish genes rx1 and rx2 help define the region of forebrain that
849 gives rise to retina. *Developmental biology* 231:13-30
850 Collantes, E.R.A., M.S. Delfin, B. Fan, J.M.R. Torregosa, C. Siguan-Bell, N.V.d.G. Florcruz, J.M.D. Martinez, B.J.
851 Masna-Hidalgo, V.P.T. Guzman, J.F. Anotado-Flores, F.D. Levina, S.R.C. Hernandez, A.A. Collantes, M.C.
852 Sibulo, S. Rong, and J.L. Wiggs. 2022. EFEMP1 rare variants cause familial juvenile-onset open-angle
853 glaucoma. *Human Mutation* 43:240-252 https://doi.org/10.1002/humu.24320.
854 Collery, R.F., K.N. Veth, A.M. Dubis, J. Carroll, and B.A. Link. 2014. Rapid, accurate, and non-invasive
855 measurement of zebrafish axial length and other eye dimensions using SD-OCT allows longitudinal
856 analysis of myopia and emmetropization. *PLoS One* 9:e110699
857 Crowley, M.A., D.L. Garland, H. Sellner, A. Banks, L. Fan, T. Rejtar, N. Buchanan, O. Delgado, Y.Y. Xu, S. Jose,
858 C.M. Adams, M. Mogi, K. Wang, C.E. Bigelow, S. Poor, K. Anderson, B.D. Jaffee, G. Prasanna, C.
859 Grosskreutz, R. Fernandez-Godino, E.A. Pierce, T.P. Dryja, and S.-M. Liao. 2022. Complement factor B
860 is critical for sub-RPE deposit accumulation in a model of Doyne honeycomb retinal dystrophy with
861 features of age-related macular degeneration. *Human Molecular Genetics* 32:204-217
862 10.1093/hmg/ddac187.
863 Daniel, S., M. Renwick, V.Q. Chau, S. Datta, P. Maddineni, G. Zode, E.M. Wade, S.P. Robertson, W.M. Petroll,
864 and J.D. Hulleman. 2020. Fibulin-3 knockout mice demonstrate corneal dysfunction but maintain
865 normal retinal integrity. *Journal of Molecular Medicine* 98:1639-1656 10.1007/s00109-020-01974-z.
866 Di Donato, V., F. De Santis, T.O. Auer, N. Testa, H. Sánchez-Iranzo, N. Mercader, J.-P. Concordet, and F. Del
867 Bene. 2016. 2C-Cas9: a versatile tool for clonal analysis of gene function. *Genome research* 26:681-
868 692
869 Ding, X., D. Fu, S. Ge, Q. Guan, M. Chen, and Z. Yu. 2020. DNA methylation and mRNA expression of IGF-1 and
870 MMP-2 after form-deprivation myopia in guinea pigs. *Ophthalmic and Physiological Optics* 40:491-501
871 https://doi.org/10.1111/opo.12696.
872 Dityatev, A., and M. Schachner. 2006. The extracellular matrix and synapses. *Cell and Tissue Research* 326:647-
873 654 10.1007/s00441-006-0217-1.
874 Driver, S.G.W., M.R. Jackson, K. Richter, P. Tomlinson, B. Brockway, B.J. Halliday, D.M. Markie, S.P. Robertson,
875 and E.M. Wade. 2020. Biallelic variants in EFEMP1 in a man with a pronounced connective tissue
876 phenotype. *European Journal of Human Genetics* 28:445-452 10.1038/s41431-019-0546-7.
877 Fischer, A.J., J.J. McGuire, F. Schaeffel, and W.K. Stell. 1999. Light- and focus-dependent expression of the
878 transcription factor ZENK in the chick retina. *Nature Neuroscience* 2:706-712 10.1038/11167.
879 Garland, D.L., R. Fernandez-Godino, I. Kaur, K.D. Speicher, J.M. Harnly, J.D. Lambris, D.W. Speicher, and E.A.
880 Pierce. 2013. Mouse genetics and proteomic analyses demonstrate a critical role for complement in a
881 model of DHRD/ML, an inherited macular degeneration. *Human Molecular Genetics* 23:52-68
882 10.1093/hmg/ddt395.
883 Gerber, D.M., F.L. Munier, and G.n. Niemeyer. 2003. Cross-sectional Study of Visual Acuity and
884 Electroretinogram in Two Types of Dominant Drusen. *Investigative Ophthalmology & Visual Science*
885 44:493-496 10.1167/iovs.01-0787.
886 Gonzalez-Fernandez, F., and D. Ghosh. 2008. Focus on molecules: interphotoreceptor retinoid-binding protein
887 (IRBP). *Experimental eye research* 86:169-170

888 Halpern, M.E., J. Rhee, M.G. Goll, C.M. Akitake, M. Parsons, and S.D. Leach. 2008. Gal4/UAS Transgenic Tools
889 and Their Application to Zebrafish. *Zebrafish* 5:97-110 10.1089/zeb.2008.0530.
890 Hayashi, K., K. Ohno-Matsui, N. Shimada, M. Moriyama, A. Kojima, W. Hayashi, K. Yasuzumi, N. Nagaoka, N.
891 Saka, T. Yoshida, T. Tokoro, and M. Mochizuki. 2010. Long-term Pattern of Progression of Myopic
892 Maculopathy: A Natural History Study. *Ophthalmology* 117:1595-1611.e1594
893 https://doi.org/10.1016/j.ophtha.2009.11.003.
894 Holden, B.A., T.R. Fricke, D.A. Wilson, M. Jong, K.S. Naidoo, P. Sankaridurg, T.Y. Wong, T.J. Naduvilath, and S.
895 Resnikoff. 2016. Global prevalence of myopia and high myopia and temporal trends from 2000
896 through 2050. *Ophthalmology* 123:1036-1042
897 Ikuno, Y. 2017. Overview of the complications of high myopia. *Retina* 37:2347-2351
898 Itoh, H., P. Keller, H. Mogami, A. Lindqvist, and R. Word. 2010. Progesterone and transforming growth factor
899 beta 1 (TGFB1) regulate matrix metalloproteinases (MMPS) in human endometrium. *Fertility and*
900 *Sterility* 94:S214
901 Jia, Y., D.-N. Hu, J. Sun, and J. Zhou. 2017. Correlations Between MMPs and TIMPs Levels in Aqueous Humor
902 from High Myopia and Cataract Patients. *Current Eye Research* 42:600-603
903 10.1080/02713683.2016.1223317.
904 Jia, Y., D.-N. Hu, D. Zhu, L. Zhang, P. Gu, X. Fan, and J. Zhou. 2014. MMP-2, MMP-3, TIMP-1, TIMP-2, and TIMP-
905 3 Protein Levels in Human Aqueous Humor: Relationship With Axial Length. *Investigative*
906 *Ophthalmology & Visual Science* 55:3922-3928 10.1167/iovs.14-13983.
907 Jobling, A.I., M. Nguyen, A. Gentle, and N.A. McBrien. 2004. Isoform-specific changes in scleral transforming
908 growth factor-β expression and the regulation of collagen synthesis during myopia progression.
909 *Journal of Biological Chemistry* 279:18121-18126
910 Kleiner, M., D. Brainard, D. Pelli, A. Ingling, R. Murray, and C. Broussard. 2007. What's new in Psychtoolbox-3.
911 *Perception* 36:1
912 Kroll, F., G.T. Powell, M. Ghosh, G. Gestri, P. Antinucci, T.J. Hearn, H. Tunbak, S. Lim, H.W. Dennis, J.M.
913 Fernandez, D. Whitmore, E. Dreosti, S.W. Wilson, E.J. Hoffman, and J. Rihel. 2021. A simple and
914 effective F0 knockout method for rapid screening of behaviour and other complex phenotypes. *eLife*
915 10:e59683 10.7554/eLife.59683.
916 Kuiper, E.J., J.M. Hughes, R.J. Van Geest, I.M.C. Vogels, R. Goldschmeding, C.J.F. Van Noorden, R.O.
917 Schlingemann, and I. Klaassen. 2007. Effect of VEGF-A on Expression of Profibrotic Growth Factor and
918 Extracellular Matrix Genes in the Retina. *Investigative Ophthalmology & Visual Science* 48:4267-4276
919 10.1167/iovs.06-0804.
920 Labun, K., T.G. Montague, M. Krause, Y.N. Torres Cleuren, H. Tjeldnes, and E. Valen. 2019. CHOPCHOP v3:
921 expanding the CRISPR web toolbox beyond genome editing. *Nucleic acids research* 47:W171-W174
922 Liu, Y., and Y. Sun. 2018. MMP-2 participates in the sclera of guinea pig with form-deprivation myopia via IGF-
923 1/STAT3 pathway. *European Review for Medical and Pharmacological Sciences* 22:2541-2548
924 Livak, K.J., and T.D. Schmittgen. 2001. Analysis of Relative Gene Expression Data Using Real-Time Quantitative
925 PCR and the 2−ΔΔCT Method. *Methods* 25:402-408 https://doi.org/10.1006/meth.2001.1262.
926 Livingstone, I., V.N. Uversky, D. Furniss, and A. Wiberg. 2020. The Pathophysiological Significance of Fibulin-3.
927 *Biomolecules* 10:1294
928 Lu, Z.-L., and B. Dosher. 2013. Visual psychophysics: From laboratory to theory. MIT Press,
929 Ma, M., Z. Zhang, E. Du, W. Zheng, Q. Gu, X. Xu, and B. Ke. 2014. Wnt signaling in form deprivation myopia of
930 the mice retina. *PLoS One* 9:e91086
931 Mackay, D.S., T.M. Bennett, and A. Shiels. 2015. Exome sequencing identifies a missense variant in EFEMP1 co-
932 segregating in a family with autosomal dominant primary open-angle glaucoma. *PloS one*
933 10:e0132529
934 Mackenzie, F., and C. Ruhrberg. 2012. Diverse roles for VEGF-A in the nervous system. *Development* 139:1371-
935 1380 10.1242/dev.072348.
936 Marcus, M.W., M.M. de Vries, F.G.J. Montolio, and N.M. Jansonius. 2011. Myopia as a Risk Factor for Open-
937 Angle Glaucoma: A Systematic Review and Meta-Analysis. *Ophthalmology* 118:1989-1994.e1982
938 https://doi.org/10.1016/j.ophtha.2011.03.012.
939 Marmorstein, L.Y., F.L. Munier, Y. Arsenijevic, D.F. Schorderet, P.J. McLaughlin, D. Chung, E. Traboulsi, and A.D.
940 Marmorstein. 2002. Aberrant accumulation of EFEMP1 underlies drusen formation in Malattia
941 Leventinese and age-related macular degeneration. *Proceedings of the National Academy of Sciences*
942 99:13067-13072 doi:10.1073/pnas.202491599.

943 McCurley, A.T., and G.V. Callard. 2008. Characterization of housekeeping genes in zebrafish: male-female
944 differences and effects of tissue type, developmental stage and chemical treatment. *BMC molecular*
945 *biology* 9:1-12
946 Najafzadeh, M.J., A. Zand, M. Shafiei, M. Sharifi, N. Nasiri, and A. Sharifi. 2023. Myopia Progression during the
947 COVID-19 Era: A Systematic Review and Meta-analysis. *Seminars in Ophthalmology* 1-10
948 10.1080/08820538.2023.2168490.
949 Quint, W.H., K.C. Tadema, E. de Vrieze, R.M. Lukowicz, S. Broekman, B.H. Winkelman, M. Hoevenaars, H.M. de
950 Gruiter, E. Van Wijk, and F. Schaeffel. 2021. Loss of Gap Junction Delta-2 (GJD2) gene orthologs leads
951 to refractive error in zebrafish. *Communications Biology* 4:676
952 Rabin, J., R.C. Van Sluyters, and R. Malach. 1981. Emmetropization: a vision-dependent phenomenon.
953 *Investigative Ophthalmology & Visual Science* 20:561-564
954 Reinhardt, R., L. Centanin, T. Tavhelidse, D. Inoue, B. Wittbrodt, J.-P. Concordet, J.R. Martinez-Morales, and J.
955 Wittbrodt. 2015. Sox2, Tlx, Gli3, and Her9 converge on Rx2 to define retinal stem cells in vivo. *The*
956 *EMBO Journal* 34:1572-1588 10.15252/embj.201490706.
957 Rio, D.C., M. Ares, G.J. Hannon, and T.W. Nilsen. 2010. Purification of RNA using TRIzol (TRI reagent). *Cold*
958 *Spring Harbor Protocols* 2010:pdb. prot5439
959 Rose, K.A., I.G. Morgan, J. Ip, A. Kifley, S. Huynh, W. Smith, and P. Mitchell. 2008. Outdoor activity reduces the
960 prevalence of myopia in children. *Ophthalmology* 115:1279-1285
961 Schindelin, J., I. Arganda-Carreras, E. Frise, V. Kaynig, M. Longair, T. Pietzsch, S. Preibisch, C. Rueden, S.
962 Saalfeld, and B. Schmid. 2012. Fiji: an open-source platform for biological-image analysis. *Nature*
963 *methods* 9:676
964 Schippert, R., E. Burkhardt, M. Feldkaemper, and F. Schaeffel. 2007. Relative Axial Myopia in Egr-1 (ZENK)
965 Knockout Mice. *Investigative Ophthalmology & Visual Science* 48:11-17 10.1167/iovs.06-0851.
966 Seko, Y., H. Shimokawa, and T. Tokoro. 1995. Expression of bFGF and TGF-beta 2 in experimental myopia in
967 chicks. *Investigative Ophthalmology & Visual Science* 36:1183-1187
968 Shand, J., K.B. Døving, and S.P. Collin. 1999. Optics of the developing fish eye: comparisons of Matthiessen's
969 ratio and the focal length of the lens in the black bream Acanthopagrus butcheri (Sparidae, Teleostei).
970 *Vision Research* 39:1071-1078 https://doi.org/10.1016/S0042-6989(98)00215-6.
971 Shi, W.-Q., T. Wan, B. Li, T. Li, and X.-D. Zhou. 2023. EFEMP1 is a potential biomarker of choroid thickness
972 change in myopia. *Frontiers in Neuroscience* 17:1144421
973 Singh, V.K., A. Mangalam, S. Dwivedi, and S. Naik. 1998. Primer premier: program for design of degenerate
974 primers from a protein sequence. *Biotechniques* 24:318-319
975 Štih, V., L. Petrucco, A.M. Kist, and R. Portugues. 2019. Stytra: An open-source, integrated system for
976 stimulation, tracking and closed-loop behavioral experiments. *PLOS Computational Biology*
977 15:e1006699 10.1371/journal.pcbi.1006699.
978 Stone, E.M., A.J. Lotery, F.L. Munier, E. Héon, B. Piguet, R.H. Guymer, K. Vandenburgh, P. Cousin, D. Nishimura,
979 R.E. Swiderski, G. Silvestri, D.A. Mackey, G.S. Hageman, A.C. Bird, V.C. Sheffield, and D.F. Schorderet.
980 1999. A single EFEMP1 mutation associated with both Malattia Leventinese and Doyne honeycomb
981 retinal dystrophy. *Nature Genetics* 22:199-202 10.1038/9722.
982 Stratikopoulos, E., M. Szabolcs, I. Dragatsis, A. Klinakis, and A. Efstratiadis. 2008. The hormonal action of IGF1
983 in postnatal mouse growth. *Proceedings of the National Academy of Sciences* 105:19378-19383
984 doi:10.1073/pnas.0809223105.
985 Tedja, M.S., A.E.G. Haarman, M.A. Meester-Smoor, J. Kaprio, D.A. Mackey, J.A. Guggenheim, C.J. Hammond,
986 V.J.M. Verhoeven, C.C.W. Klaver, and f.t.C. Consortium. 2019. IMI – Myopia Genetics Report.
987 *Investigative Ophthalmology & Visual Science* 60:M89-M105 10.1167/iovs.18-25965.
988 Tedja, M.S., R. Wojciechowski, P.G. Hysi, N. Eriksson, N.A. Furlotte, V.J. Verhoeven, A.I. Iglesias, M.A. Meester-
989 Smoor, S.W. Tompson, and Q. Fan. 2018. Genome-wide association meta-analysis highlights light-
990 induced signaling as a driver for refractive error. *Nature genetics* 50:834
991 Troilo, D., M.D. Gottlieb, and J. Wallman. 1987. Visual deprivation causes myopia in chicks with optic nerve
992 section. *Current eye research* 6:993-999
993 Turnbull, P.R.K., S. Backhouse, and J.R. Phillips. 2015. Visually guided eye growth in the squid. *Current Biology*
994 25:R791-R792 10.1016/j.cub.2015.07.073.
995 Wallman, J., M.D. Gottlieb, V. Rajaram, and L.A. Fugate-Wentzek. 1987. Local retinal regions control local eye
996 growth and myopia. *Science* 237:73-77
997 Wisard, J., A. Faulkner, M.A. Chrenek, T. Waxweiler, W. Waxweiler, C. Donmoyer, G.I. Liou, C.M. Craft, G.F.
998 Schmid, J.H. Boatright, M.T. Pardue, and J.M. Nickerson. 2011. Exaggerated Eye Growth in IRBP-

Deficient Mice in Early Development. *Investigative Ophthalmology & Visual Science* 52:5804-5811 10.1167/iovs.10-7129.

Xie, J., P.T. Goodbourn, B.V. Bui, and P.R. Jusuf. 2023. Establishment and comprehensive characterization of a novel dark-reared zebrafish model for myopia studies. *bioRxiv* doi.org/10.1101/2023.11.19.567749 (Preprint posted November 21, 2023).

Xie, J., P.T. Goodbourn, B.V. Bui, T.E. Sztal, and P.R. Jusuf. 2019a. Correspondence Between Behavioral, Physiological, and Anatomical Measurements of Visual Function in Inhibitory Neuron–Ablated Zebrafish. *Investigative ophthalmology & visual science* 60:4681-4690

Xie, J., P.R. Jusuf, B.V. Bui, S. Dudczig, T.E. Sztal, and P.T. Goodbourn. 2021. Altered Visual Function in a Larval Zebrafish Knockout of Neurodevelopmental Risk Gene pdzk1. *Investigative Ophthalmology & Visual Science* 62:29-29 10.1167/iovs.62.3.29.

Xie, J., P.R. Jusuf, B.V. Bui, and P.T. Goodbourn. 2019b. Experience-dependent development of visual sensitivity in larval zebrafish. *Scientific Reports* 9:1-11

Xie, J., P.R. Jusuf, P.T. Goodbourn, and B.V. Bui. 2019c. Electroretinogram Recording in Larval Zebrafish using A Novel Cone-Shaped Sponge-tip Electrode. *JoVE* e59487 10.3791/59487.

Yang, T., H. Zhang, H. Qiu, B. Li, J. Wang, G. Du, C. Ren, and X. Wan. 2016. EFEMP1 is repressed by estrogen and inhibits the epithelial-mesenchymal transition via Wnt/β-catenin signaling in endometrial carcinoma. *Oncotarget* 7:25712

Yue, B. 2014. Biology of the extracellular matrix: an overview. *Journal of glaucoma* S20

Zhang, J., S. Bai, C. Tanase, H. Nagase, and M.P. Sarras. 2003. The expression of tissue inhibitor of metalloproteinase 2 (TIMP-2) is required for normal development of zebrafish embryos. *Development Genes and Evolution* 213:382-389 10.1007/s00427-003-0333-9.

Zhu, X., S. Dellostritto, A. Nour, and A. Benavente-Perez. 2021. Vascular Endothelial Growth Factor-A (VEGF-A) and High Myopia in Marmosets. *Investigative Ophthalmology & Visual Science* 62:2875-2875